UPPSALA
UNIVERSITET

Digital Comprehensive Summaries of Uppsala Dissertations from the Faculty of Science and Technology 721

Density Functional Theory Applied to Materials for Spintronics

DIANA MIHAELA IUŞAN

ACTA
UNIVERSITATIS
UPSALIENSIS
UPPSALA
2010

ISSN 1651-6214
ISBN 978-91-554-7737-0
urn:nbn:se:uu:diva-119887

Dissertation presented at Uppsala University to be publicly examined in Polhemsalen, 751 20 Uppsala, Ångström Laboratory, Friday, April 16, 2010 at 10:15 for the degree of Doctor of Philosophy. The examination will be conducted in English.

Abstract
Iuşan, D M. 2010. Density Functional Theory Applied to Materials for Spintronics. Acta Universitatis Upsaliensis. *Digital Comprehensive Summaries of Uppsala Dissertations from the Faculty of Science and Technology* 721. 67 pp. Uppsala. ISBN 978-91-554-7737-0.

The properties of dilute magnetic semiconductors have been studied by combined *ab initio*, Monte Carlo, and experimental techniques. This class of materials could be very important for future spintronic devices, that offer enriched functionality by making use of both the spin and the charge of the electrons. The main part of the thesis concerns the transition metal doped ZnO.

The role of defects on the magnetic interactions in Mn-doped ZnO was investigated. In the presence of acceptor defects such as zinc vacancies and oxygen substitution by nitrogen, the magnetic interactions are ferromagnetic. For dilute concentrations of Mn (~ 5%) the ordering temperature of the system is low, due to the short ranged character of the exchange interactions and disorder effects.

The clustering tendency of the Co atoms in a ZnO matrix was also studied. The electronic structure, and in turn the magnetic interactions among the Co atoms, is strongly dependent on the exchange-correlation functional used. It is found that Co impurities tend to form nanoclusters and that the interactions among these atoms are antiferromagnetic within the local spin density approximation + Hubbard *U* approach.

The electronic structure, as well as the chemical and magnetic interactions in Co and (Co,Al)-doped ZnO, was investigated by joined experimental and theoretical techniques. For a good agreement between the two, approximations beyond the local density approximation must be used. It is found that the Co atoms prefer to cluster within the semiconducting matrix, a tendency which is increased with Al co-doping. We envision that it is best to describe the system as superparamagnetic due to the formation of Co nanoclusters within which the interactions are antiferromagnetic.

The magnetic anisotropy and evolution of magnetic domains in $Fe_{81}Ni_{19}$/Co(001) superlattices were investigated both experimentally, as well as using model spin dynamics. A magnetic reorientation transition was found.

Keywords: spintronics, dilute magnetic semiconductors, density functional theory, exchange interactions, magnetic percolation, ordering temperature, disorder, electronic structure

Diana Mihaela Iuşan, Department of Physics and Astronomy, Materials Theory, Box 516, Uppsala University, SE-751 20 Uppsala, Sweden

ISSN 1651-6214
ISBN 978-91-554-7737-0
urn:nbn:se:uu:diva-119887 (http://urn.kb.se/resolve?urn=urn:nbn:se:uu:diva-119887)

To my family

Cover illustration:
An artist's view of the world of spintronics. Designed and drawn by Ilie Bucşa at the indications of the author.

List of Papers

This thesis is based on the following papers, which are referred to in the text by their Roman numerals.

I **Theoretical study of the magnetism of Mn-doped ZnO with and without defects**
D. Iuşan, B. Sanyal, and O. Eriksson
Physical Review B **74**, 235208 (2006)

II **Role of defects on the magnetic interactions in Mn-doped ZnO**
D. Iuşan, B. Sanyal, and O. Eriksson
Physica Status Solidi A **204**, 53 (2007)

III **Influence of defects on the magnetism of Mn-doped ZnO**
D. Iuşan, B. Sanyal, and O. Eriksson
Journal of Applied Physics **101**, 09H101 (2007)

IV **Ordering in diluted magnetic semiconductors: A magnetic percolation phenomenon**
O. Eriksson, D. Iuşan, R. Knut, and B. Sanyal
Journal of Applied Physics **101**, 09H114 (2007)

V **Microscopic picture of Co clustering in ZnO**
D. Iuşan, M. Kabir, O. Grånäs, O. Eriksson, and B. Sanyal
Physical Review B **79**, 125202 (2009)

VI **Inhomogeneity in Co doped ZnO diluted magnetic semiconductor**
B. Sanyal, R. Knut, O. Grånäs, D. M. Iuşan, O. Karis, and O. Eriksson
Journal of Applied Physics **103**, 07D131 (2008)

VII **Electronic structure and chemical and magnetic interactions in ZnO doped with Co and Al: Experiments and *ab initio* density-functional calculations**
D. Iuşan, R. Knut, B. Sanyal, O. Karis, O. Eriksson, V. A. Coleman, G. Westin, J. M. Wikberg, and P. Svedlindh
Physical Review B **78**, 085319 (2008)

VIII **Electronic structure of Co doped ZnO: Theory and experiment**
B. Sanyal, O. Grånäs, R. Knut, V. A. Coleman, P. Thunström, D. M. Iuşan, O. Karis, O. Eriksson, and G. Westin
Journal of Applied Physics **103**, 07D130 (2008)

IX **Magnetic anisotropy and evolution of ground-state domain structures in bcc $Fe_{81}Ni_{19}$/Co(001) superlattices**
R. Bručas, H. Hafermann, I. L. Soroka, D. Iuşan, B. Sanyal, M. I. Katsnelson, O. Eriksson, and B. Hjörvarsson
Physical Review B **78**, 024421 (2008)

X **Competing anisotropies in bcc $Fe_{81}Ni_{19}$/Co(001) superlattices**
H. Hafermann, R. Bručas, I. L. Soroka, M. I. Katsnelson, D. Iuşan, B. Sanyal, O. Eriksson, and B. Hjörvarsson
Applied Physics Letters **94**, 073102 (2009)

The following papers are co-authored by me but are not included in this Thesis.

- **Effect of diffusion and alloying on the magnetic and transport properties of Fe/V/Fe trilayers**
  D. Iuşan, M. Alouani, O. Bengone O, and O. Eriksson
  Physical Review B **75**, 024412 (2007)

- **Competing exchange interactions in magnetic multilayers**
  B. Skubic, E. Holmström, D. Iuşan, O. Bengone, O. Eriksson, R. Brucas, H. Hjörvarsson, V. Stanciu, and P. Nordblad
  Physical Review Letters **96**, 057205 (2006)

- **Ab-initio computational modeling of complex magnetism in spintronic materials**
  B. Sanyal, D. M. Iuşan, R. Knut, O. Grånäs, and O. Eriksson
  AIP Conference Proceedings **1003**, 230 (2008), Magnetic Materials: International Conference on Magnetic Materials (ICMM-2007)

Contents

Introduction

Conventional electronic devices are based on the electrical transport of charge carriers, the electrons, through a semiconductor, typically silicon-based. Spintronics, on the other hand, envisions using both the charge and the spin of the electrons, thus closing the gap between the semiconducting and magneto-recording industries. This leads to a new generation of devices which, although smaller, are thought to be able to handle more information than the conventional ones.

The pioneering discovery in the field of spintronics was the giant magnetoresistance (GMR) effect by Albert Fert and Peter Grünberg in 1988, for which the scientists were awarded the Nobel Prize in Physics in 2007. The effect consists in a very large change in the electrical resistance when a magnetic field is applied, and it is due to the spin-dependent transport of the electrons. It took less than 10 years for this discovery to become materialized in the computer industry. Nowadays personal computers are the norm, their size has shrunk, and their speed has increased considerably over the last decade, still keeping the prices at bay. Together with the internet, it has affected the way we work, use our phones, interact in general. But this would be the subject of a thesis in itself.

A particular group of materials which have caught on in the field of spintronics are dilute magnetic semiconductors (DMS). As the same suggest, they consist of a semiconducting matrix into which a small amount of magnetic impurities is introduced. For practical applications, it is desired to find DMS in which the magnetic spins order above room temperature. The schematic representation of such a materials is shown in Fig. 1.

An encouraging moment came in 1992, when Hideo Ohno and his colleagues discovered ferromagnetism in indium arsenide (InAs) containing only 1.3% manganese (Mn) [1]. A few years later, in 1996, they have indicated ferromagnetic ordering in Mn-doped gallium arsenide (GaAs) as well, with a ordering temperature of 110 K [2]. Subsequent works report an ordering temperature for this system as high as 173 K [3], probably the largest unquestionable value for this class of materials as for now. Another influential work was the one of Tomasz Dietl which, by means of model theory, predicted the ordering temperatures of a series of Mn-doped semiconductors [4]. According to this model, Mn-doped zinc oxide (ZnO) or gallium nitride (GaN) could have a ferromagnetic ordering temperature as high as 300 K. These findings have triggered an immense interest in these materials, leading to thousands

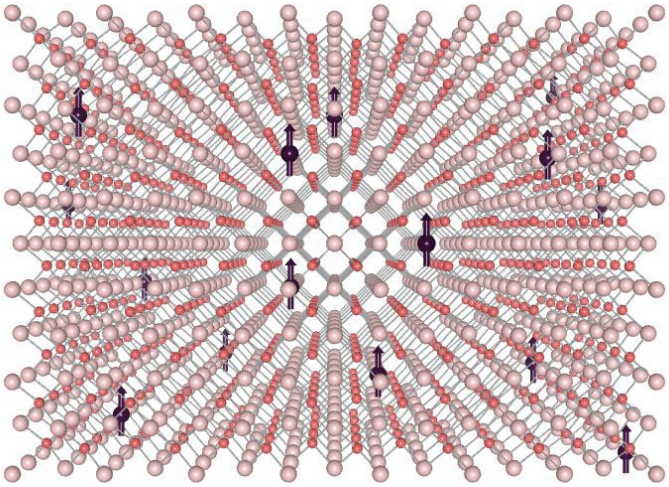

Figure 1: Schematic representation of a dilute magnetic semiconductor.

of articles, a number which is still increasing. Despite this, the magnetism of these materials continues to be a matter of controversy, and no unanimous ordering temperature well above room temperature has been established.

This thesis tackles the magnetism of dilute magnetic semiconductors from an *ab initio* point of view. In order to determine materials properties, density functional theory (DFT)-based computations have been performed. DFT transforms the complicated many-body problem of the electrons into a simpler one that requires only the knowledge of the distribution of the electron charge in space. The foundations of the theory were set by Pierre Hohenberg and Walter Kohn in 1964. It soon became a very popular technique and it was successfully applied to a wide range of materials. Due to its versatility in calculating properties of materials, one of its founders, Walter Kohn, was awarded the Nobel Prize in Chemistry in 1998. In order to study the properties of the materials at different temperatures, we have combined DFT with Monte Carlo simulations. From these, we can trace the variation of the magnetization with temperature and determine the transition temperature of the system.

We have applied this machinery to a series of dilute magnetic semiconductors. Their magnetic properties have been related to the details of the electronic structure.

The thesis is organized as follows: In part I we describe the computational methods used in our studies. Part II contains a short description of the results obtained. For more details, the Reader is directed to the original papers attached.

Part I:
Theoretical Methods

1. Density Functional Theory

The goal of condensed matter physics is to determine the properties of solids, and one way of doing so is to calculate the electronic structure. The knowledge of the electronic structure of solids is not only helpful for the understanding and explanation of experiments, but most important, it allows the prediction of properties of newly designed materials.

1.1 The Many-Body Problem

In order to determine the properties of a system, one needs to solve the Schrödinger equation

$$H_t \Psi = E_{tot} \Psi, \tag{1.1}$$

where H_t is the Hamiltonian describing all the interactions of the system, E_{tot} is the total energy of the system, and Ψ is the many-body wave function containing all the information that can be obtained about the nuclei and electrons in the system. The full Hamiltonian can be expressed as

$$\begin{aligned} H = T + T_n + V_{int} + V_{nn} + V_{ext} = -\frac{\hbar^2}{2m_e} \sum_i \nabla_i^2 - \sum_I \frac{\hbar^2}{2M_I} \nabla_I^2 \\ + \frac{1}{2} \sum_{i \neq j} \frac{e^2}{|\mathbf{r}_i - \mathbf{r}_j|} + \frac{1}{2} \sum_{I \neq J} \frac{Z_I Z_J e^2}{|\mathbf{R}_I - \mathbf{R}_J|} - \sum_{i,I} \frac{Z_I e^2}{|\mathbf{r}_i - \mathbf{R}_I|}, \end{aligned} \tag{1.2}$$

where m_e and $\mathbf{r}_i$ are the electron mass and positions, M_I are the masses of the nuclei, R_I the corresponding positions, and Z_I is the nuclear charge. The first two terms in eq. (1.2) are the kinetic energy of the electrons, T, and the kinetic energy of the nuclei, T_n. The following terms correspond to the potential energy: V_{int} is the electron-electron repulsion term, V_{nn} is the nuclei-nuclei repulsion term, and V_{ext} is the attractive interaction term between the electrons and the nuclei, described as an external potential for the electrons. The summations in the expression run over all the electrons and the nuclei in the system.

Because the mass of the nuclei is much larger than the mass of the electrons, the kinetic energy of the nuclei can be neglected in comparison to the kinetic energy of the electrons. This leads us to the Born-Oppenheimer approximation [5], which allows us to simplify the problem by considering the nuclei at fixed positions and treating only the motion of the electrons in a crystal potential.

The Hamiltonian for the electrons becomes

$$H_e = T + V_{int} + V_{ext} = -\frac{\hbar^2}{2m_e}\sum_i \nabla_i^2 - \sum_{i,I}\frac{Z_I e^2}{|\mathbf{r}_i - \mathbf{R}_I|} + \frac{1}{2}\sum_{i\neq j}\frac{e^2}{|\mathbf{r}_i - \mathbf{r}_j|}. \tag{1.3}$$

The many-body wave function is now dependent only on the coordinates and spins of electrons, the coordinates of the nuclei entering only as parameters.

Even within the Born-Oppenheimer approximation, the number of particles (electrons) entering the problem is of the order 10^{23}, making an exact solution impossible. Therefore, one needs to appeal to further approximations in order to make the problem solvable.

1.2 The Hohenberg-Kohn Theorems

A popular technique for solving the electronic structure problem is density functional theory (DFT). Within the DFT, the complicated many-body motion of all electrons is replaced by an equivalent but simpler problem of a single electron moving in an effective potential. The fundamentals of this theory are set in two papers, the first one by Hohenberg and Kohn in 1964 [6] and the follow-up by Kohn and Sham in 1965 [7]. The main idea of this theory is to replace the complicated wave function by the electron density, $n(\mathbf{r})$.

Density functional theory is based on the theorems:

Theorem 1 The potential V_{ext} of a system (and thus the Hamiltonian and the total energy) is determined uniquely, up to constant, by the ground state density $n(\mathbf{r})$.

Theorem 2 The total energy functional $E[n]$, for a given V_{ext}, is minimized by the ground state density $n(\mathbf{r})$.

The total energy of the system can then be written as a functional of density

$$E[n] = \int d^3r V_{ext}(\mathbf{r})n(\mathbf{r}) + F[n], \tag{1.4}$$

where V_{ext} is the external potential due to the interaction with the nuclei. $F[n]$ is a functional containing the kinetic energy and the electron-electron interactions. The form of this functional is not known and one needs to adopt schemes for obtaining an expression for it that can later be used in the computations.

1.3 The Kohn-Sham Equations

The Kohn-Sham scheme relies on the assumption that there exists a non-interacting system which has the same ground state density $n(\mathbf{r})$ as the interacting system.

Then, the Kohn-Sham functional can be written as

$$E[n] = \int d^3r V_{ext}(\mathbf{r})n(\mathbf{r}) + T_s[n] + E_{xc}[n] + \frac{e^2}{2}\int\int d^3r d^3r' \frac{n(\mathbf{r})n(\mathbf{r}')}{|\mathbf{r}-\mathbf{r}'|}, \tag{1.5}$$

where T_s is the kinetic energy of the non-interacting electrons. The last term is the so-called Hartree term, $E_{Hartree}[n]$, and it represents the classical Coulomb interaction energy of the electron density $n(\mathbf{r})$.
The term $E_{xc}[n]$ is the exchange-correlation density functional. It contains contributions from the exchange and correlation energy of the interacting system and it contains the difference in the kinetic energy between the non-interacting system and the interacting system.

Minimizing eq. (1.5) with respect to $n(\mathbf{r})$, and demanding a stationary solution, leads us to a Schrödinger-like equation for the Kohn-Sham system:

$$\left[-\frac{\hbar^2}{2m_e}\nabla^2 + V_{eff}(\mathbf{r})\right]\psi_i(\mathbf{r}) = \epsilon_i\psi_i(\mathbf{r}), \tag{1.6}$$

where ϵ_i are the eigenvalues and $\psi_i(\mathbf{r})$ are the Kohn-Sham orbitals for the non-interacting electrons. V_{eff} is the effective potential

$$V_{eff}(\mathbf{r}) = V_{ext}(\mathbf{r}) + e^2\int \frac{n(\mathbf{r}')}{|\mathbf{r}-\mathbf{r}'|}d^3r' + V_{xc}(\mathbf{r}), \tag{1.7}$$

where V_{xc} is the exchange-correlation potential determined by the functional derivative

$$V_{xc}(\mathbf{r}) = \frac{\partial E_{xc}[n]}{\partial n}. \tag{1.8}$$

The electron density, $n(\mathbf{r})$, can be written in terms of the Kohn-Sham orbitals as

$$n(\mathbf{r}) = \sum_{i}^{occ.} |\psi_i(\mathbf{r})|^2, \tag{1.9}$$

where the summation runs over all occupied states.

In computations the electron density is calculated iteratively. One starts from an initial guess, which is used to construct the effective potential via eq. (1.7). Then the Kohn-Sham eigenvalue problem, eq. (1.6), is solved and

the occupied states are used to create a new electron density, eq. (1.9). From it, a new effective potential is constructed until self-consistency is reached.

The kinetic energy of the non-interacting electrons is given by

$$T_s[n] = \sum_i \epsilon_i - \int d^3r V_{eff}(\mathbf{r}) n(\mathbf{r}). \tag{1.10}$$

The total energy of the interacting system can then be written as

$$E[n] = \sum_i^{occ.} \epsilon_i - E_{Hartree} - \int d^3r V_{xc}(\mathbf{r}) n(\mathbf{r}) + E_{xc}[n]. \tag{1.11}$$

1.4 The Exchange-Correlation Functional

All the unknowns of the problem are now collected in the exchange-correlation term, which is unknown and must be approximated. A first suggestion was the local density approximation (LDA) [7, 8]. Within this approximation, the exchange-correlation term is expressed as

$$E_{xc}^{LDA}[n] = \int d^3r n(\mathbf{r}) \varepsilon_{xc}(n(\mathbf{r})), \tag{1.12}$$

where $\varepsilon_{xc}(n(\mathbf{r}))$ is the exchange-correlation energy per particle for a homogeneous electron gas with density $n(\mathbf{r})$.

The quantity $\varepsilon_{xc}(n(\mathbf{r}))$ can be split into two, the exchange and the correlation contributions, as

$$\varepsilon_{xc}(n(\mathbf{r})) = \varepsilon_x(n(\mathbf{r})) + \varepsilon_c(n(\mathbf{r})). \tag{1.13}$$

The exchange part of a homogeneous electron gas can be calculated from the Hartree-Fock method [9] and is given by

$$\varepsilon_x(n(\mathbf{r})) = -\frac{3}{4} e^2 \left(\frac{3}{\pi}\right)^{1/3} (n(\mathbf{r}))^{1/3}. \tag{1.14}$$

The correlation part, $\varepsilon_c(n(\mathbf{r}))$, is more difficult to calculate. Accurate results have been obtained by using the quantum Monte Carlo method [10]. Based on these results, several parametrizations for the exchange-correlation functional have been proposed [11, 12].

The LDA has been very successful in describing ground state properties of a large number of physical systems. It is best suited in treating materials with small variations in the electronic density. When there are strong gradients, due

to directional bonding for example, the LDA is less good. Also, the band gaps in semiconductors and insulators are usually underestimated by 40 %.

There have been several attempts to improve upon the LDA. In the generalized gradient approximation (GGA) [13], the exchange-correlation potential depends both on the density and its gradient: $\varepsilon[n, |\nabla n|]$. The self-interaction corrected (SIC) methods [14, 15] try to improve the LDA by removing the self-interaction term in the electrostatic and exchange-correlation energy. The SIC-LDA is successful in treating f-electron materials and transition metal oxides [16]. Another scheme is the LDA+U [17], which includes the on-site Coulomb interaction (U) for the description of correlation effects in localized d- and f-bands.

1.5 The Bloch Theorem and Basis Sets

The one-electron problem, eq. (1.6) $-$ (1.9), can be greatly simplified if the crystal has a periodic structure, i.e., the effective potential is periodic

$$V_{eff}(\mathbf{r} + \mathbf{T}) = V_{eff}(\mathbf{r}), \tag{1.15}$$

where $\mathbf{T}$ is a translational vector of the lattice. If this condition is fulfilled, then the *Bloch theorem* states that the wave function can be written as

$$\psi_{\mathbf{k}}(\mathbf{r}) = exp(i\mathbf{k} \cdot \mathbf{r}) u_{\mathbf{k}}(\mathbf{r}), \tag{1.16}$$

where $u_{\mathbf{k}}$ is a function having the periodicity of the crystal lattice. Therefore, it is sufficient to find the wave function only in the primitive cell.

In order to solve the Kohn-Sham equation, eq. (1.6), we can expand the one-electron wave functions as

$$\psi_{n\mathbf{k}}(\mathbf{r}) = \sum_i c_{i,n\mathbf{k}} \chi_{i\mathbf{k}}(\mathbf{r}), \tag{1.17}$$

where $\chi_{i,\mathbf{k}}$ forms a complete set of basis functions and satisfies the Bloch condition, eq. (1.16), and n is the band index.

The coefficients $c_{i,n\mathbf{k}}$ are obtained from

$$\sum_j [< \chi_{i\mathbf{k}}|H|\chi_{j\mathbf{k}} > - \epsilon_{n\mathbf{k}} < \chi_{i\mathbf{k}}|\chi_{j\mathbf{k}} >] c_{j,n\mathbf{k}} = 0, \tag{1.18}$$

where $< \chi_{i\mathbf{k}}|H|\chi_{j\mathbf{k}} >$ are the matrix elements for the effective Hamiltonian and $< \chi_{i\mathbf{k}}|\chi_{j\mathbf{k}} >$ are elements for the overlap matrix.

The energies $\epsilon_{n\mathbf{k}}$ are determined from the secular equation:

$$det[< \chi_{i\mathbf{k}}|H|\chi_{j\mathbf{k}} > - \epsilon_{n\mathbf{k}} < \chi_{i\mathbf{k}}|\chi_{j\mathbf{k}} >] = 0. \tag{1.19}$$

There are various methods for solving the electronic structure problem, depending on the choice of the *basis functions* χ_i, such as: the augmented (APW) or orthogonalized (OPW) plane waves, linear muffin-tin orbitals (LMTO), linear combination of atomic orbitals (LCAO), etc. Among others are the Korringa-Kohn-Rostoker method and the pseudopotential approach.

2. Computational Methods

2.1 The Projector Augmented Wave Method

The numerical difficulties in solving the Kohn-Sham equation (1.6) come from the very different signatures of the wave functions in different regions in space:

- In the atomic region around the nucleus, the wave functions present rapid oscillations, which require fine grids for accurate numerics. However, the wave functions can be expressed by a small basis set, such as one consisting of atomic-like orbitals.
- In the bonding region between the atoms, on the contrary, the wave functions have smooth variations. Nevertheless, the wave function is very susceptible to changes in the environment, therefore large basis sets are required.

The strategy of the augmented wave methods is to divide the space into atom-centered spheres, where the basis set consists of atomic-like wave functions, and the interstitial region in between, where the wave functions are expanded into plane waves or another convenient basis set. The partial solutions of the different regions are later matched at the boundary between the atomic and interstitial regions.

The projector augmented wave method (PAW) [18] is an all-electron method inspired from the augmented wave methods, but has a twist to it. This consists of a linear transformation of the true Kohn-Sham wave functions with their complete nodal structure onto computationally convenient wave functions. Let us denote the physical one-electron wave functions by $|\psi_n\rangle$ and their "transformed" ones by $|\widetilde{\psi}_n\rangle$, which we will call from now on pseudo wave functions. Then

$$|\psi_n\rangle = \mathcal{T}|\widetilde{\psi}_n\rangle, \tag{2.1}$$

where $\mathcal{T}$ is to be defined. The variational principle with respect to the pseudo wave functions yields

$$\mathcal{T}^\dagger H \mathcal{T}|\widetilde{\psi}_n\rangle = \mathcal{T}^\dagger \mathcal{T}|\widetilde{\psi}_n\rangle \epsilon_n, \tag{2.2}$$

where H is the Kohn-Sham Hamiltonian.

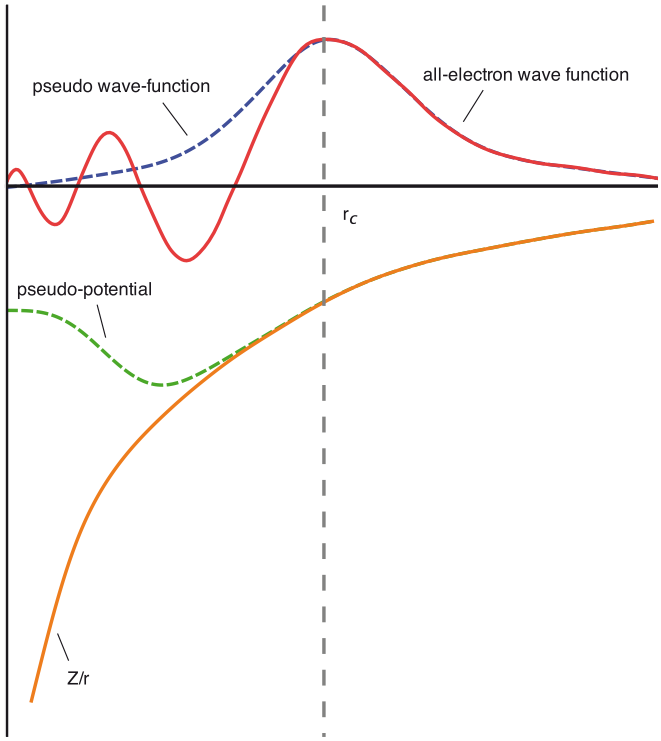

Figure 2.1: Schematic illustration of an atomic all-electron wave function (red line) and the corresponding atomic pseudo wave function (blue line), as well as the Coulomb potential (orange line) and pseudopotential (green line).

As the pseudo wave functions are intended to avoid the complicated nodal structure around the nuclei, the linear transformation $\mathcal{T}$ is constructed as a sum of local atom-centered transformations that differ from unity only within some augmentation regions $\Omega_{\mathbf{R}}$ ($\mathbf{R}$ – atomic site) enclosing the atoms

$$\mathcal{T} = 1 + \sum_{\mathbf{R}} \mathcal{T}_{\mathbf{R}}. \tag{2.3}$$

So, by construction, the all-electron and the pseudo wave functions coincide outside the augmentation regions, as illustrated in Fig. 2.1.

The terms $\mathcal{T}_{\mathbf{R}}$ are defined in terms of the functions $|\phi_i\rangle$, which are chosen as the solutions of the Schrödinger equation for the isolated atoms and orthogonal to the core states if necessary. Namely:

$$|\phi_i\rangle = \left(1 + \sum_{\mathbf{R}} \mathcal{T}_{\mathbf{R}}\right) |\widetilde{\phi}_i\rangle \qquad \text{within } \Omega_{\mathbf{R}}. \tag{2.4}$$

The initial states $|\widetilde{\phi}_i\rangle$ are called pseudo partial waves and the corresponding target functions $|\phi_i\rangle$ all-electron partial waves. The index i refers to the atomic site $\mathbf{R}$, the angular momentum quantum numbers $L = (l, m)$, and an additional index α to label different partial waves for the same site and angular momentum.

Within the augmentation region every pseudo wave function $|\widetilde{\psi}\rangle$ can be expanded into pseudo partial waves:

$$|\widetilde{\psi}\rangle = \sum_i |\widetilde{\phi}_i\rangle c_i \qquad \text{within } \Omega_{\mathbf{R}}. \tag{2.5}$$

The corresponding all-electron wave function has the form

$$|\psi\rangle = \mathcal{T}|\widetilde{\psi}\rangle = \sum_i |\phi_i\rangle c_i \qquad \text{within } \Omega_{\mathbf{R}}. \tag{2.6}$$

Therefore, the all-electron wave functions can be written as

$$|\psi\rangle = |\widetilde{\psi}\rangle - \sum_i |\widetilde{\phi}_i\rangle c_i + \sum_i |\phi_i\rangle c_i. \tag{2.7}$$

As $\mathcal{T}$ is a linear transformation, the coefficients c_i are defined as the scalar products

$$c_i = \langle \tilde{p}_i | \widetilde{\psi} \rangle, \tag{2.8}$$

where $\langle \tilde{p}_i|$ is a projector function which fulfills the completeness relation

$$\sum_i |\widetilde{\phi}_i\rangle \langle \tilde{p}_i| = 1 \tag{2.9}$$

and the orthogonality relation

$$\langle \tilde{p}_i | \widetilde{\phi}_j \rangle = \delta_{ij}. \tag{2.10}$$

Physical quantities of interest are obtained from the expectation values of the corresponding operators. Given an operator A, its expectation value is

$\langle A \rangle = \sum_n f_n \langle \psi_n | A | \psi_n \rangle$, where f_n is the occupation number of a state n. Alternatively, it can be calculated as $\langle A \rangle = \sum_n f_n \langle \widetilde{\psi}_n | \tilde{A} | \widetilde{\psi}_n \rangle$, where $\tilde{A} = \mathcal{T}^\dagger A \mathcal{T}$ acts as on the pseudo wave functions. For a quasi-local operator:

$$\tilde{A} = A + \sum_{ij} |\tilde{p}_i\rangle \left(\langle \phi_i | A | \phi_j \rangle - \langle \widetilde{\phi}_i | A | \widetilde{\phi}_j \rangle \right) \langle \tilde{p}_j |. \tag{2.11}$$

Adding a term of the form

$$B - \sum_{ij} |\tilde{p}_i\rangle \langle \widetilde{\phi}_i | B | \widetilde{\phi}_j \rangle \langle \tilde{p}_j |, \tag{2.12}$$

where B is located within the augmentation region, does not change the expectation value of the operator $\tilde{A}$. This can be used in order to avoid the singularity of the Coulomb potential at the nuclear site (*see* Fig. 2.1) and to obtain an expression that is less sensitive to the truncation of number of plane waves.

The charge density at a point r in space is given by the expectation value of the projection operator $|r\rangle\langle r|$. Following eq. (2.11) we obtain:

$$n(r) = \tilde{n}(r) + n^1(r) - \tilde{n}^1(r), \tag{2.13}$$

where

$$\tilde{n}(r) = \sum_n f_n \langle \widetilde{\psi}_n | r \rangle \langle r | \widetilde{\psi}_n \rangle, \tag{2.14}$$

$$n^1(r) = \sum_{n,(i,j)} f_n \langle \widetilde{\psi}_n | \tilde{p}_i \rangle \langle \phi_i | r \rangle \langle r | \phi_j \rangle \langle \tilde{p}_j | \widetilde{\psi}_n \rangle, \tag{2.15}$$

and

$$\tilde{n}^1(r) = \sum_{n,(i,j)} f_n \langle \widetilde{\psi}_n | \tilde{p}_i \rangle \langle \widetilde{\phi}_i | r \rangle \langle r | \widetilde{\phi}_j \rangle \langle \tilde{p}_j | \widetilde{\psi}_n \rangle. \tag{2.16}$$

The terms $n^1(r)$ and $\tilde{n}^1(r)$ are localized around each atom and can be calculated in spherical coordinates.

The PAW method is exact within the DFT framework, provided the plane-wave expansion is complete and the partial wave expansion in eq. (2.5) is converged. Typically, one or two partial waves per angular momentum (l, m) and site are used. Part of the results presented in this thesis were obtained by using the PAW methos as implemented in the Vienna Ab Initio Simulation Package (VASP) [19, 20].

2.2 The KKR-ASA Method

An alternative way of solving the Kohn-Sham problem (1.6) is the Korringa-Kohn-Rostoker method [21, 22]. There are nowadays several implementations of the method, assuming different degrees of approximations.

One common approximation is to consider that the effective potential has the so-called muffin-tin form, that consists of spherically symmetric parts within the muffin-tin spheres located at the atomic sites and a constant potential, the muffin-tin zero, V_{MTZ}, in the interstitial region between the spheres. Thus, the potential at site $\mathbf{R}$, $V_{MT}(r_{\mathbf{R}})$, can be written as

$$V_{MT}(r_{\mathbf{R}}) = \begin{cases} V(r_{\mathbf{R}}) - V_{MTZ} & r \leq S_{MT} \\ 0 & r > S_{MT}, \end{cases} \tag{2.17}$$

where $V(r_{\mathbf{R}})$ is the spherically symmetric potential and S_{MT} is the muffin-tin sphere at site $\mathbf{R}$.

The Schrödinger equation for the muffin-tin potential at site $\mathbf{R}$ is

$$\left[-\nabla^2 + V_{MT}(r_{\mathbf{R}})\right] \varphi_{\mathbf{R}L}(\epsilon, r) = \epsilon \varphi_{\mathbf{R}L}(\epsilon, r). \tag{2.18}$$

Due to the spherical symmetry of the muffin-tin potential, the wave function inside the muffin-tin sphere can be written as a product of a radial function $\varphi_{\mathbf{R}l}(\epsilon, r)$ and a function dependent on angular momentum:

$$\varphi_{\mathbf{R}L}(\epsilon, \mathbf{r}) = i^l \varphi_{\mathbf{R}l}(\epsilon, r) Y_l^m(\hat{\mathbf{r}}), \tag{2.19}$$

with $L = (l, m)$. The radial part $\varphi_{\mathbf{R}l}(\epsilon, r)$ satisfies the radial Schrödinger equation

$$\left[-\frac{d^2}{dr^2} + \frac{l(l+1)}{r^2} + V_{MT}(r_{\mathbf{R}}) - \epsilon\right] \varphi_{\mathbf{R}l}(\epsilon, r) = 0. \tag{2.20}$$

Outside the muffin-tin (in the interstitial region), where the potential is constant, the solution is a linear combination of spherical Bessel $J_L(\epsilon, r)$ and Neumann $K_L(\epsilon, r)$ functions.

The KKR method can be further combined with the *atomic sphere approximation* (ASA) [23, 24]. Within the ASA, the radius of the muffin-tin sphere S_{MT} is chosen to be equal to the Wigner-Seitz radius S_{WS}. This implies that the muffin-tin spheres are now space-filling and overlap with each other. Also, the kinetic energy in the interstitial region is chosen to be zero. As a consequence, the functions J_L and K_L are no longer energy dependent.

The basis functions needed to solve the Kohn-Sham problem are chosen as muffin-tin orbitals. Due to their smart construction, a minimal number is

needed for accurate calculations. In the ASA, the muffin-tin orbitals have the simplified form [25]:

$$\chi_{\mathbf{R}L}(\epsilon,\mathbf{r}) = \begin{cases} N_{\mathbf{R}L}(\epsilon)\varphi_{\mathbf{R}L}(\phi,\mathbf{r}) + P_{\mathbf{R}l}(\epsilon)J_L(\mathbf{r}_\mathbf{R}) & r \leq S_{MT} \\ K_L(\mathbf{r}_\mathbf{R}) & r > S_{MT}, \end{cases} \tag{2.21}$$

where $N_{\mathbf{R}l}(\epsilon)$ is the so-called normalization function

$$N_{\mathbf{R}l}(\epsilon) = (2l+1)\frac{1}{\varphi_{\mathbf{R}l}(S_{MT},\epsilon)}\frac{1}{l - D_{\mathbf{R}l}(\epsilon)}, \tag{2.22}$$

$P_{\mathbf{R}l}(\epsilon)$ is the potential function:

$$P_{\mathbf{R}l}(\epsilon) = 2(2l+1)\frac{D_{\mathbf{R}l}(\epsilon) + L + 1}{D_{\mathbf{R}l}(\epsilon) - 1} \tag{2.23}$$

and $D_{\mathbf{R}l}(\epsilon)$ is the logarithmic derivative of $\chi_{\mathbf{R}L}(\epsilon,\mathbf{r})$ at the sphere boundary, given by

$$D_{\mathbf{R}l}(\epsilon) = \left.\frac{S_{MT}}{\varphi_{\mathbf{R}l}(\epsilon,r)}\frac{\partial\varphi_{\mathbf{R}l}(\epsilon,r)}{\partial r}\right|_{r=S_{MT}}. \tag{2.24}$$

By construction, the muffin-tin orbital is continuous and differentiable in all space.

The irregular solutions, $K_L(\mathbf{r}_\mathbf{R})$, at site $\mathbf{R}$ can be expanded in terms of the regular solutions $J_L(\mathbf{r}_{\mathbf{R}'})$, at another site $\mathbf{R}'$

$$K_L(\mathbf{r}_\mathbf{R}) = -\sum_{L'} S_{\mathbf{R}L,\mathbf{R}'L'}J_{L'}(\mathbf{r}_{\mathbf{R}'}), \tag{2.25}$$

where $\mathbf{R} \neq \mathbf{R}'$ and $S_{\mathbf{R}L,\mathbf{R}'L'}$ are the *s*tructure constants, which only depend on the crystal lattice.

The Schrödinger equation inside an atomic sphere is fulfilled provided that the tails from all the other sites of the lattice cancel out the second term ($r \leq S_{MT}$) in eq. (2.21).

We consider a linear expansion

$$\psi_i(\mathbf{r}) = \sum_{\mathbf{R}L} a_{i,\mathbf{R}L}\chi_{\mathbf{R}L}(\epsilon,\mathbf{r}) \tag{2.26}$$

of the Kohn-Sham eigenstates, $\psi_i(\mathbf{r})$, in terms of muffin-tin orbitals $\chi_{\mathbf{R}L}(\epsilon,\mathbf{r})$. The *tail cancellation* condition can be written as

$$\sum_{\mathbf{R}L} a_{i,\mathbf{R}L}[P_{\mathbf{R}l}(\epsilon)\delta_{\mathbf{R}L,\mathbf{R}'L'} - S_{\mathbf{R}L,\mathbf{R}'L'}] = 0. \tag{2.27}$$

Non-trivial solutions for the set of linear equations (2.27) exist only if the secular determinant vanishes:

$$\det\left[P_{\mathbf{R}l}(\epsilon)\delta_{\mathbf{R}L,\mathbf{R}'L'} - S_{\mathbf{R}L,\mathbf{R}'L'}\right] = 0, \tag{2.28}$$

which yields the energy spectrum of the Schrödinger equation in the ASA. The secular equation indicates that the electronic structure problem has separated into two parts: (i) the potential functions $P_{\mathbf{R}l}$ that describe the properties of the atomic spheres and (ii) the structure constants $S_{\mathbf{R}L,\mathbf{R}'L'}$ that contain the information about the positions of the atomic spheres.

For a periodic lattice, the KKR-ASA equation can be Fourier transformed, resulting in a secular equation in the reciprocal space

$$\det\left[P_l(\epsilon)\delta_{LL'} - S_{LL'}(\mathbf{k})\right] = 0, \tag{2.29}$$

where **k** is a vector in the Brillouin zone.

2.3 The Green's Function Formalism

The KKR method, also called multiple scattering theory, can also be described by using an equivalent formalism based on Green's functions. As the wave function, the Green's function contains all the information related to the system, and, once known, can be used to calculate any physical quantity.

The Green's function $G(\mathbf{r}, \mathbf{r'}; \epsilon)$ describes the propagation of an independent particle (electron) from a position **r** to a position **r'**, at an energy ϵ, and satisfies the Schrödinger-like equation

$$\left[-\frac{\hbar^2}{2m_e}\nabla^2_{\mathbf{r}} - (\epsilon - V_{eff}(\mathbf{r}))\right] G(\mathbf{r} - \mathbf{r'}; \epsilon) = -\delta(\mathbf{r} - \mathbf{r'}) \tag{2.30}$$

The crystal is be viewed as a collection of scatterers at the atomic sites. The single scattering events from any of the atoms in the crystal are represented by the on-site matrix elements t. If G_0 is a reference Green function, the free-particle propagator, for example, then the full Green's function can be written as

$$\begin{aligned} G_0 &= G_0 + G_0 t G_0 + G_0 t G_0 t G_0 = \dots \\ &= G_0 + tG \\ \Rightarrow G &= \left({G_0}^{-1} - t\right)^{-1} \end{aligned} \tag{2.31}$$

Similarly, one can write G as

$$G = G_0 + G_0 T G_0, \tag{2.32}$$

where T is the full scattering matrix of the system.

The stationary states of the system are given by the poles of G or T as a function of ϵ and are obtained from the zeroes of the determinant

$$\det\left(t^{-1} - G_0\right) = 0. \tag{2.33}$$

In the KKR-ASA method, the role of t^{-1} is played by the potential function, while G_0 corresponds to the structure constants. Also, an auxiliary Green's function is introduced

$$g(\mathbf{k}, z) = \left[P_l(z) - S(\mathbf{k})\right]^{-1}, \tag{2.34}$$

from which the full Green function can be calculated, z being the complex energy.

Given the Green's function, the local density of states can be calculated as

$$n_L(\mathbf{r}, z) = -\frac{1}{\pi} \text{ Im } G_{LL}(\mathbf{r}, \mathbf{r}; z) \tag{2.35}$$

and the total density:

$$n(\mathbf{r}) = -\frac{1}{\pi} \int_{-\infty}^{E_F} dz \sum_L \text{ Im } G_{LL}(\mathbf{r}, \mathbf{r}; z). \tag{2.36}$$

2.4 The Coherent Potential Approximation

The coherent potential approximation (CPA) in the single-site approximation is a method for treating substitutionally random alloys [26, 27, 28]. Let us assume for simplicity that the alloy consists of two types of atoms (A and B). The idea behind the CPA is to replace the random configuration of atoms by effective atoms that describe the average properties of the system (like the total energy, the density of states, the on-site Green's function). These atoms represent the *effective medium*. When inserted in this medium, the A

and B atoms are treated as impurities. The unknown effective medium is then determined from the condition of vanishing average scattering resulting from embedding a single impurity, A or B, with probabilities $c_A = c$ and $c_B = 1 - c$, into the effective medium. This implies the following condition for the auxiliary Green's function

$$\tilde{g}_{\mathbf{R}L,\mathbf{R}L'} = c g^{A}_{\mathbf{R}L,\mathbf{R}L'} + (1-c) g^{B}_{\mathbf{R}L,\mathbf{R}L'}, \tag{2.37}$$

where $\tilde{g}_{\mathbf{R}L,\mathbf{R}L'}$ is the auxiliary Green's function for the effective medium and $g^{A,B}_{\mathbf{R}L,\mathbf{R}L'}$ are the auxiliary Green's functions for the embedded atoms A and B in the effective medium.

$\tilde{g}_{\mathbf{R}L,\mathbf{R}L'}$ can be written as

$$\tilde{g}_{\mathbf{R}L,\mathbf{R}L'} = \frac{1}{V_{BZ}} \int_{BZ} \left[\tilde{P}_{\mathbf{R}l} - S_{\mathbf{R}L,\mathbf{R}L'} \right]^{-1} d\mathbf{k}, \tag{2.38}$$

where $\tilde{P}_{\mathbf{R}l}$ is the *coherent potential function* that describes the properties of the effective, non-random atoms which characterize the system after configurational averaging.

The Green's functions of the embedded atoms A and B are

$$g^{A,B}_{\mathbf{R}L,\mathbf{R}L'} = \frac{1}{1 + \tilde{g}_{\mathbf{R}L,\mathbf{R}L'} \left[P^{A,B}_{\mathbf{R}l} - \tilde{P}_{\mathbf{R}l} \right]} \tilde{g}_{\mathbf{R}L,\mathbf{R}L'}. \tag{2.39}$$

Combining equations (2.37) and (2.39), we get to the following expression for the coherent potential function of the effective medium

$$\tilde{P}_{\mathbf{R}l} = c P^{A}_{\mathbf{R}l} + (1-c) P^{B}_{\mathbf{R}l} + \left[P^{A}_{\mathbf{R}l} - \tilde{P}_{\mathbf{R}l} \right] \tilde{g}_{\mathbf{R}L,\mathbf{R}L'} \left[P^{B}_{\mathbf{R}l} - \tilde{P}_{\mathbf{R}l} \right]. \tag{2.40}$$

The coherent potential function is not a self-averaging quantity, as it is not just a linear combination of the two element specific potential functions $P^{A}_{\mathbf{R}l}$ and $P^{B}_{\mathbf{R}l}$.

The essence of the single-site approximation consists in a complete neglect of local environmental effects and a site-diagonal character of the coherent potential function. But despite the lack of including local environmental effects and cluster effects, the CPA describes generally well the composition trends of the ground state properties, such as total energies, lattice constants, local densities of states, and related quantities. A method going beyond the CPA is the embedded cluster method (ECM) [29].

3. Magnetism at Finite Temperatures

The quantitative description of finite-temperature properties of magnetic systems has been a challenge for solid-state theorists for decades. Due to the implementation of practical schemes for solving the band structure, such as density functional theory, there is nowadays a good understanding of the ground state properties (i.e., at $T = 0K$). Although DFT can be extended to finite temperatures [30], there is at present no practical scheme for its implementation. Therefore, one needs to rely on approximations or assumptions based on physical arguments.

The magnetic excitations in ferromagnets are of two types:

1. *Stoner excitations*, in which an electron is excited from an occupied state of the majority-spin band to an empty state of the minority-spin band. They correspond to longitudinal fluctuations of the magnetization.

2. *Spin waves or magnons*, which correspond to collective transverse fluctuations of the direction of the magnetization.

In the low-temperature regime, the Stoner excitations can be neglected in comparison to the magnons. It is reasonable to extend this approximation up to the Curie temperature, and to evaluate it by neglecting the Stoner excitations. This is a good approximation for ferromagnets with a large exchange splitting, such as dilute magnetic semiconductors.

We can therefore adopt the *adiabatic approximation*, in which the precession of the magnetization due to a spin wave is neglected when calculating the associated change of the electronic energy. In other words, the motion of the electrons is assumed to be much faster than the change in the magnetic moments.

In order to determine the thermodynamic properties we follow a two-step approach [31, 32]. The *first step* is determining self-consistently the electronic structure at zero temperature using density functional methods. The total energy is then mapped to an effective Heisenberg Hamiltonian with classical spins

$$H = -\sum_{i \neq j} J_{ij} \mathbf{S}_i \cdot \mathbf{S}_j, \tag{3.1}$$

where $\mathbf{S}_i$ and $\mathbf{S}_j$ denote the local moments of the atoms at sites i and j and J_{ij} is the exchange integral between these atoms. The *second step* is resolving

the effective Hamiltonian by statistical methods in order to obtain the Curie temperature.

3.1 Heisenberg Exchange Parameters

There are two approaches to calculate the exchange interaction parameters. The first one is the real-space approach. The exchange parameters J_{ij} are calculated directly from the energy change associated with a constrained rotation of mgnetic moments at sites i and j [33]. By employing the magnetic force theorem [33, 34, 35], the change of the total energy of the system can be approximated by the corresponding change of one-particle energies.

Within the Green's function formalism, the formula for pair-exchange parameters reads

$$J_{ij} = \frac{1}{4\pi} \int^{E_F} dE \; Im \; Tr_L(\Delta_i T_{\uparrow}^{ij} \Delta_j T_{\downarrow}^{ji}), \tag{3.2}$$

where $\Delta_i = t_{i\uparrow}^{-1} - t_{i\downarrow}^{-1}$, t being the on-site scattering matrix. T is the scattering path operator which is related to the off-diagonal element of the Green's function. Tr_L is the trace over the orbital indices of the scattering matrices. A positive (negative) J_{ij} represents ferromagnetic (antiferromagnetic) interaction.

The second approach for calculating the exchange parameters is the frozen-magnon approach [36, 37]. It is a reciprocal-space method based on spin spirals. The frozen-magnon approach is preferred for the calculations of magnon spectra, while the real-space approach is more suitable for the calculations of exchange interactions.

3.2 Spin-Wave Stiffness Constant

The spin-wave coefficient *D* can be calculated from the exchange parameters as

$$D = \frac{2\mu_B}{3M} \sum_j J_{0j} R_{0j}^2. \tag{3.3}$$

The summation is over all sites R_{0j} but in practice it is performed up to a maximal value $\mathrm{R}_{\max}$.

3.3 Transition Temperatures

Once the exchange parameters are calculated, there are different approaches for obtaining the Curie temperature. One of them is the common mean-field approximation (MFA). The expression for the T_C in the MFA of the Heisenberg model is

$$T_C^{MFA} = \frac{2x}{3k_B} \sum_{j \neq 0} J_{0j}, \tag{3.4}$$

where x is the concentration of magnetic impurities and k_B is the Boltzmann constant.

Another approach is the random phase approximation (RPA) [38]. It has the advantage of correctly describing the collective excitations (spin waves) and, in general, gives a better estimate of T_C compared to the MFA.

A numerical exact solution can be obtained by using the Monte Carlo method for solving the Heisenberg Hamiltonian, eq. (3.1). In the simulations, different algorithms may be used, like the heat-bath method or the single-flip Metropolis algorithm. The critical temperature can be obtained from the forth-order cumulant crossing method [39]. The fourth order cumulant of the order parameter (magnetization) M reads

$$U_L = 1 - \frac{< M^4 >}{3 < M^2 >^2}. \tag{3.5}$$

From the intersection point of the curves of U_L for different system size L, the critical temperature is obtained.

In Paper I, the Curie temperatures in the dilute limit was also estimated using a modified form of eq. (3.4). In this approximation, $\mathrm{T_C}$ is calculated by using the value of the exchange parameter corresponding to the average distance between the magnetic spins in the expression for the mean field solution of the Heisenberg model:

$$T_C^{AMFA} = \frac{2}{3k_B} J_{<0j>}, \tag{3.6}$$

where $< 0j >$ corresponds to the *average* distance between the magnetic atoms, which is determined by their concentration.

Part II:
Summary of the Papers

4. Mn-doped ZnO

The role of defects on the magnetic properties of Mn-doped ZnO has been presented in Papers I−IV. The studies were motivated by the conflicting experimental situation regarding the magnetism of this system. Different behaviors have been reported experimentally, ranging from paramagnetism [40, 41], spin-glass [42], ferromagnetism at low temperatures [43], or even room temperature ferromagnetism [44, 45].

The electronic structure calculations were done by means of the Korringa-Kohn-Rostoker method, within the atomic sphere approximation. The chemical and magnetic disorder in the system were treated using the coherent potential approximation. The magnetic exchange parameters were calculated using Liechtenstein's theory, as described in Chapter 3. The calculated exchange interactions were used in evaluating the Curie temperature, either in a mean-field fashion, or via Monte Carlo simulations.

4.1 Crystal Structure

Although Mn-doped ZnO crystalizes in the wurtzite structure, for simplicity we have considered the zinc-blende structure in the calculations, illustrated in Fig. 4.1. Nevertheless, the values of the exchange interactions for the two structures have been compared and found not to vary substantially.

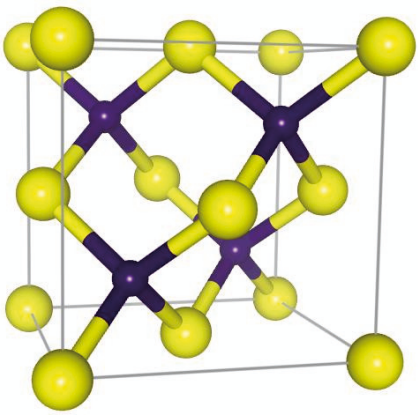

Figure 4.1: The zinc-blende structure.

4.2 Pure Mn-doped ZnO

The calculated density of states (DOS) of defect-free $Mn_{0.05}Zn_{0.95}O$ is shown in Fig. 4.2a. When Mn substitutes Zn in ZnO, it attains a 2+ charge state. This means that the electronic configuration consists of half-filled d states (d^5), and there are no free carriers introduced in the system. The local environment of the Mn atoms gives rise to a crystal field splitting of the $3d$ states into the doubly degenerate e_g states and the triply degenerate t_{2g} states. The spin-splitting of the bands is much larger than the crystal field splitting, and consequently Mn is in a high spin state.

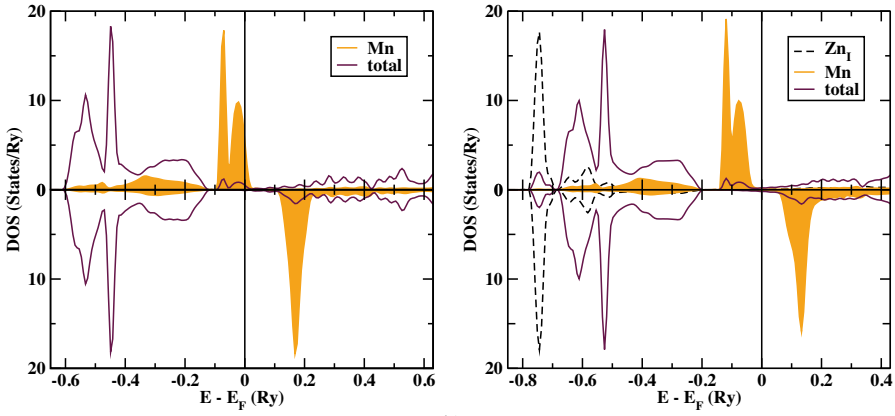

Figure 4.2: Calculated DOS of $Mn_{0.05}Zn_{0.95}O$, defect-free (a) and with 5% Zn_I incorporated (b). The total DOS is represented by a solid line, the Mn states are in orange, and the Zn_I states are presented with a dashed line. Note that the total DOS and the impurity states are not shown on the same intensity scale.

In Fig. 4.3a we show the calculated exchange interactions among the Mn atoms as a function of Mn-Mn distance, for different Mn concentrations. The magnetic interactions are antiferromagnetic (corresponding to negative values of J_{0j}) and are very strong for the nearest-neighbors. Their strength increases with increasing Mn concentration. The interactions die off exponentially with distance, as expected for magnetic interactions of magnetic elements in a semiconductor host [46]. It is worth pointing out that the exchange interactions have a strong directional dependence. Due to this it is not appropriate to use theoretical methods that approximate the exchange interactions in dilute magnetic semiconductors with an isotropic parametrized form. Antiferromagnetic interactions between Mn atoms in ZnO have also been reported experimentally [47, 48, 49].

4.3 Role of Defects

The growth of ZnO can be accompanied by the formation of defects or defect complexes. This has motivated us to study the effects of defects on the electronic structure of Mn-doped ZnO, and thus the magnetic interactions. The most common donor defects are oxygen vacancies (V_O) and zinc interstitials (Zn_I). Acceptor defects are zinc vacancies (V_{Zn}) and oxygen interstitials (O_I) [50].

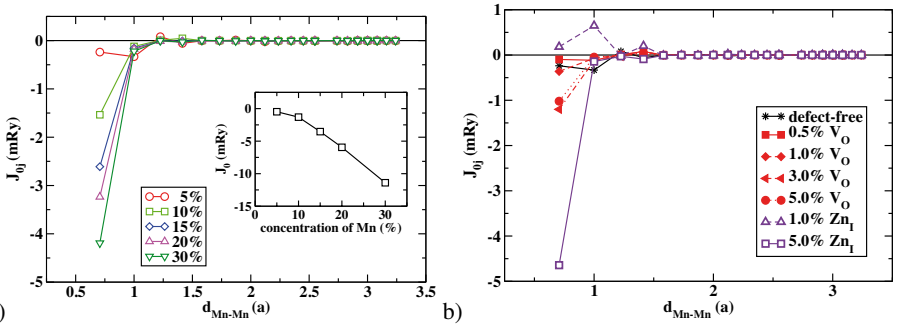

Figure 4.3: Calculated dependence of the Heisenberg exchange parameters on the distance among the magnetic atoms for various concentrations of Mn in defect-free $Mn_xZn_{1-x}O$ (a) and for different concentrations of Zn_I or V_O in $Mn_{0.05}Zn_{0.95}O$ (b). The inset in figure (a) presents the variation of $J_0 = \sum_{j\neq 0} J_{0j}$ as a function of Mn content in pure $Mn_xZn_{1-x}O$.

Donor defects

Fig. 4.2b presents the density of states of $Mn_{0.05}Zn_{0.95}O$ doped with 5% Zn_I. The change in the band structure of Mn-doped ZnO due to Zn_I can be approximated by a rigid band model where the Fermi level is simply shifted up in energy as the concentration of Zn_I increases. The calculated exchange interactions among the Mn atoms are represented in Fig. 4.3b, as a function of distance. The dominating interaction corresponds to the one among the nearest-neighbors, which is strongly antiferromagnetic: $J_{01} \simeq$ -4.5 mRy for 5% Zn_I.

In the presence of V_O defects, the exchange interactions are still antiferromagnetic (*see* Fig. 4.3b), although the effect is less pronounced compared to Zn_I.

Acceptor defects

Fig. 4.4a presents the variation of the chemical exchange parameters for $Mn_{0.05}Zn_{0.95}O$ as function of Mn-Mn separation for different concentrations of Zn vacancies. The *p*-type doping with V_{Zn} leads to ferromagnetic interactions among the Mn spins. The interactions are strongest for around

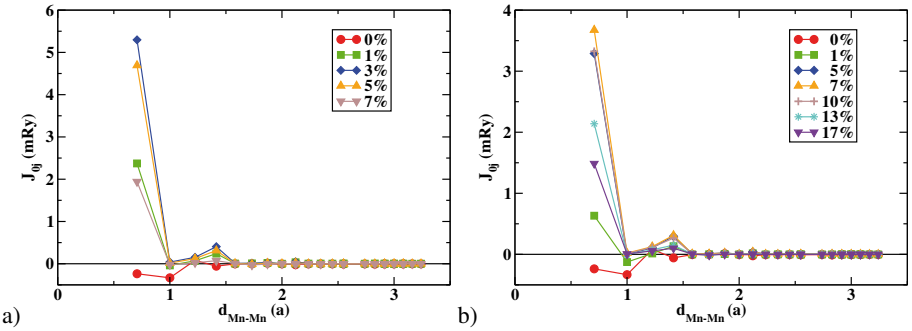

Figure 4.4: Calculated Heisenberg exchange parameters versus $\mathrm{d_{Mn-Mn}}$ for various concentrations of zinc vacancies (a) or nitrogen doping (b) in the $\mathrm{Mn_{0.05}Zn_{0.95}O}$-based system.

3% $\mathrm{V_{Zn}}$ and are again dominated by the nearest-neighbor interaction. In this case $\mathrm{J_{01}}$ is as high as 5.5 mRy, which is to be considered a very strong ferromagnetic interaction.

In order to illustrate the effect that $\mathrm{V_{Zn}}$ has on the electronic structure, we show in Fig. 4.5a the DOS of 5% Mn-doped ZnO with 5% $\mathrm{V_{Zn}}$. With increasing the concentration of $\mathrm{V_{Zn}}$, the Mn *d*-levels broaden and move down in energy.

For defect-free Mn-doped ZnO the magnetic interactions are dominated by the superexchange interaction, which is antiferromagnetic for the half-filled Mn *d*-shell. When holes are introduced, by zinc vacancies for example, the double exchange mechanism becomes dominant, giving rise to ferromagnetic interactions [51].

We have also investigated the effect of N-codoping on the magnetic interactions (denoted $\mathrm{N_O}$). Having one electron less compared to O, nitrogen acts as an acceptor when substituting oxygen in ZnO. This means that N creates holes in the system, as it can also be deduced from Fig. 4.5b, that represents the calculated DOS for the $\mathrm{Mn_{0.05}Zn_{0.95}O_{0.93}N_{0.07}}$ system. The N *2p*-states overlap in energy with the Mn *3d* $\uparrow$ states, causing them to hybridize strongly. The presence of the holes in the system stabilizes the ferromagnetic state, in a way similar to zinc vacancies.

Fig. 4.4b shows the exchange interactions between the Mn atoms for different N concentrations in $\mathrm{Mn_{0.05}Zn_{0.95}O_{1-x}N_x}$. The maximum of the nearest-neighbors interactions $\mathrm{J_{01}}$ corresponds to a N concentration of around 7%.

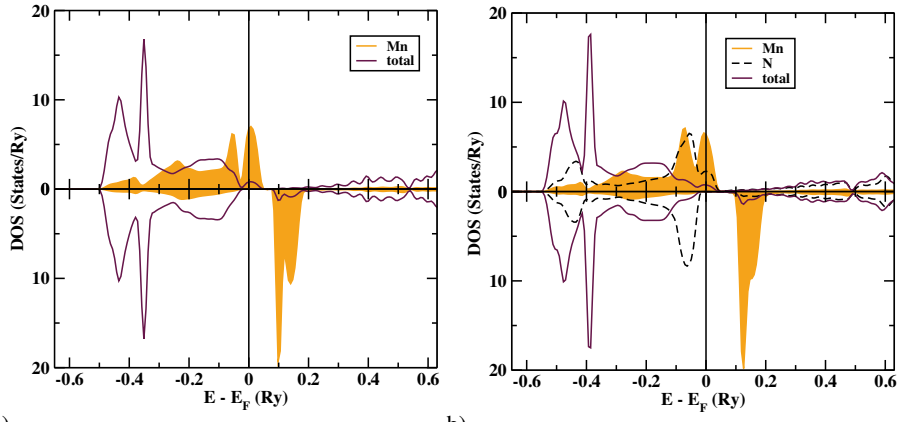

a) b)

Figure 4.5: Calculated DOS of $Mn_{0.05}Zn_{0.95}O$, for a concentration of Zn vacancies of 5% (a) and for a concentration of N of 7% (b). The total DOS is represented by a solid line, the Mn states are in orange, and the N states are represented by a dashed line. Note that the total DOS and the impurity states are not shown on the same intensity scale.

4.4 Ordering Temperatures

For the defects where ferromagnetic interactions have been found (V_{Zn} and N_O) we have evaluated the Curie temperatures, by both Monte Carlo simulations and the *average* mean-field approximation, described in section 3.3. The results are presented in Fig. 4.6. The curves obtained by these two methods are quantitatively similar, including the positions of the maxima and the order of magnitude of the critical temperatures; in contrast to the conventional mean-field approximation, eq. (3.4), that yields values which are one order of magnitude too large. Irrespective of the defects and concentration considered, the Curie temperatures of the $Mn_{0.05}Zn_{0.95}O$-based system is below 50 K. This is due to the short-range character of the exchange interactions and the low Mn concentration of 5% (below the percolation limit for a nearest-neighbor model).

Higher values of the Curie temperatures can be obtained by increasing the Mn concentration, as Fig. 4.7 depicts. Nevertheless, this needs to be combined with an increase in the number of holes, provided by either V_{Zn} or N_O, to counteract the otherwise antiferromagnetic interactions among the Mn spins. Delicately tuning the concentrations of the magnetic impurities and the holes, temperatures as high as 135 K can be obtained (*see* Fig. 4.7).

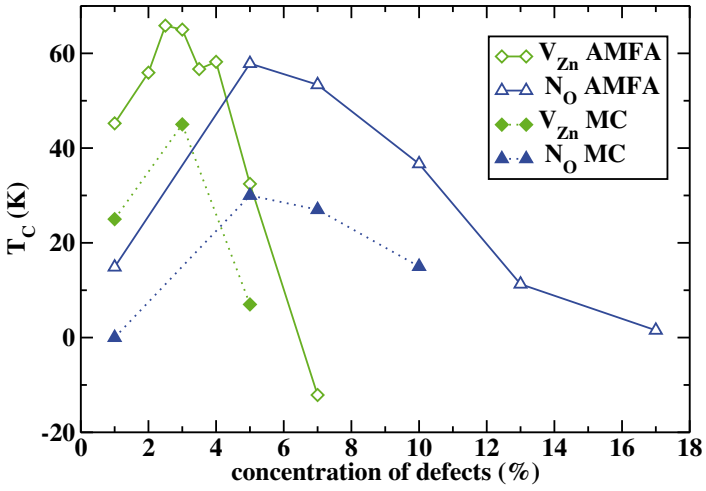

Figure 4.6: Curie temperatures calculated as a function of defect concentration by AMFA and MCS for two different types of defects for $Mn_{0.05}Zn_{0.95}O$-based systems.

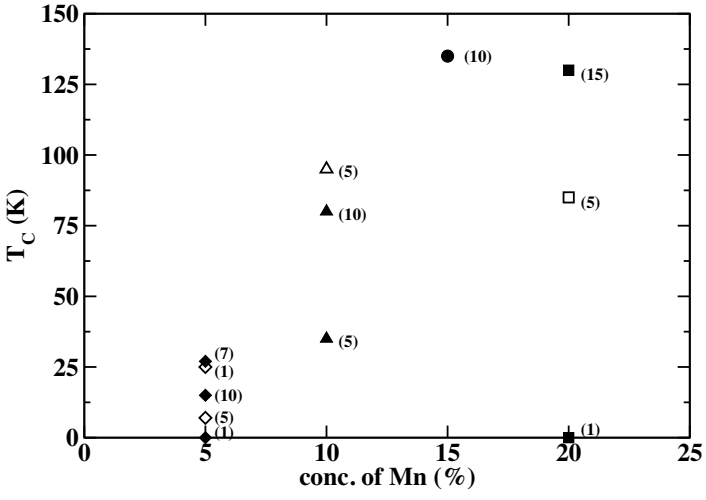

Figure 4.7: Calculated Curie temperatures by Monte Carlo simulations. Solid symbols correspond to N substitution, while open symbols are for V_{Zn}. In the parenthesis the concentration of defects is given.

5. Co-doped ZnO

Another intriguing case of a dilute magnetic semiconductor is the one of Co-doped ZnO, presented in Papers V−VI. The studies address an important problem of dilute magnetic semiconductors: namely, how the spacial arrangement of the magnetic dopants within the semiconducting matrix affect the interactions among them.

The results in Paper V were obtained by using the PAW method and the Perdew-Burke-Ernzerhof exchange-correlation functional [52]. The effect of strong electron-electron interactions were taken into account using the LSDA+U method [53].

In order to test the structural stability of the Co clusters in ZnO, supercells of different sizes were considered, in which the size of the clusters was ranged from 1 to 4. For each of the supercells considered, different arrangements of the Co atoms, as well as magnetic configurations have been investigated. The structures are illustrated in Fig. 5.1 (a)-(h), where the ground state magnetic structure for various cluster geometries is indicated.

5.1 Magnetic Interactions

From the total energies of different configurations we can determine the strength of the magnetic pair interactions, J_{ij}, between two Co atoms at sites i and j, assuming an Ising Hamiltonian. The dominant interactions correspond to the ones among the nearest-neigbors and depend on the orientation within the wurtzite lattice. Let us denote by in-plane and out-of-plane the two configurations represented in Fig. 5.1(b) and 5.1(c), respectively. The calculated values are presented in Table 5.1. Firstly, it is observed that the exchange-correlation functional used is crucial for the determination of the exchange parameters. Within the LSDA, the in-plane interactions are antiferromagnetic and increase in strength as the cluster size increases. The out-of-plane interactions are ferromagnetic for the dimer and turn antiferromagnetic for larger clusters. The situation is different within the LSDA+U, the strength of the interactions is more or less constant for different cluster sizes, and antiferromagnetic for both the in-plane and out-of-plane configurations.

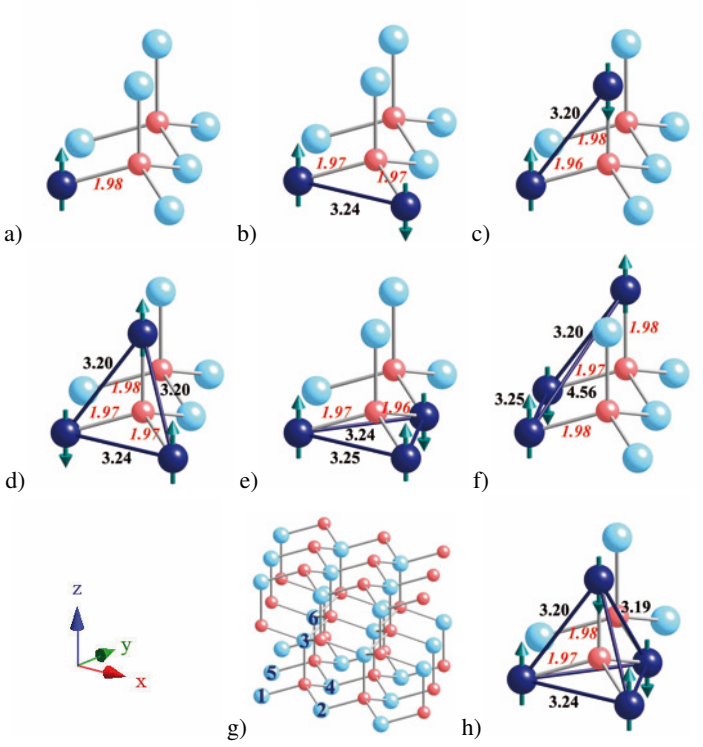

Figure 5.1: Schematic illustrations of the Co clusters in the ZnO matrix for various cluster sizes and configurations. Co, Zn and O atoms are shown as blue, turquoise and red colored balls, respectively. The bond lengths calculated by the LSDA+U method are shown. Magnetic configurations are evident from the arrows positioned on the Co atoms.

Experimentally, values of J_{in} = -21 K and J_{out} = -9 K for the exchange interactions have been reported, which are in quite good agreement with our LSDA+U values.

5.2 Electronic Structure

In order to point out the differences in the electronic structure as the size of the Co clusters increases, as well as the effect of the exchange-correlation functional, we present in Fig. 5.2 the calculated density of states for the monomer and the tetramer, both within the LSDA and LSDA+U. The effect of U is to push the Co *3d* majority bands lower in energy. Also the e_g-like peak in the minority band is moved to the top of the valence band. The system is in a half-metallic state in the LSDA case, therefore the ferromagnetic double exchange is the dominating part to the magnetic exchange. Within LSDA+U,

Table 5.1: *Exchange interaction parameters of an Ising Hamiltonian describing the magnetic interactions among the Co atoms within the cluster.*

	J (K)	dimer	trimer	tetramer
LSDA	J_{in}	-45	-59	-74
	J_{out}	22	-1	-14
LSDA+U	J_{in}	-29	-29	-30
	J_{out}	-11	-11	-12

the states around E_F are redistributed and superexchange dominates in this case. By comparing the calculated valence band spectrum with the measured one, we conclude that LSDA+U provides a better description of the electronic structure than LSDA does.

With increasing cluster size, the width of the Co bands increases. Also, the electronic structure of the O atom within the cluster changes, as a new peak appears below the Fermi level. Due to the hybridization between the O and Co atoms, a peak is induced into the Co states as well. This change in the electronic structure can be observed by looking at the magnetization density for this energy interval, shown in Fig. 5.3 and 5.4, for the monomer and tetramer, respectively. The Co states have an e_g-like character, and this is not changed by variations in the cluster size. The Co states induce a spin polarization on the neighboring O atoms. When the Co atoms cluster, the $2p$ states of the mediating O are perturbed, and the induced spin polarization of this atom is inverted (for this energy interval).

5.3 Clustering Tendency

The formation energy of the clusters can be calculated as

$$E^f = E[\mathrm{Co}_m\mathrm{Zn}_{N-m}\mathrm{O}_N] - N * E[\mathrm{ZnO}] - m * \{\mu[\mathrm{Co}] - \mu[\mathrm{Zn}]\},$$

where *m* and *N* are the number of Co and O atoms respectively, and μ is the chemical potential, corresponding to the hcp bulk systems. If E^f is positive, it means it costs energy to substitute Zn for Co in the ZnO system. The results are plotted in Fig. 5.5. The formation energy (within LSDA) shows a steady decrease, which is an indication that the Co atoms prefer to cluster. Similar trends have been observed for Cr atoms in a GaN matrix [54].

An alternative way of investigating the clustering tendency is presented in Paper VI. The chemical interactions were calculated by means of the generalized perturbation method [55]:

$$V_{ij} = V_{ij}^{\mathrm{Co-Co}} - 2V_{ij}^{\mathrm{Co-Zn}} + V_{ij}^{\mathrm{Zn-Zn}},$$

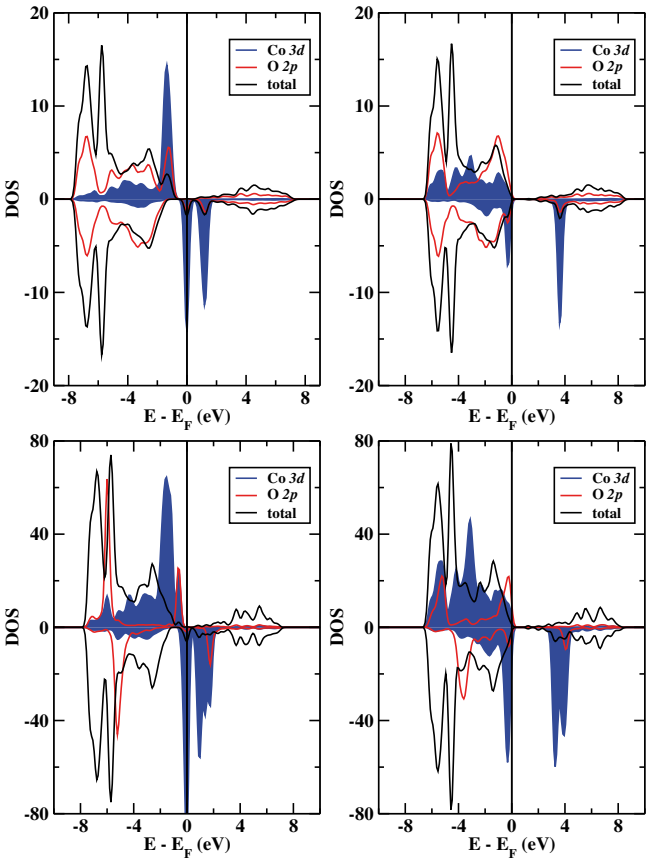

Figure 5.2: Calculated DOS for the (upper panel) Co monomer in the (left) LSDA and (right) LSDA+U and the same for (bottom panel) Co tetramer. The solid black line represents the total DOS, the blue shaded line stands for the Co *3d* states, while the red line is for the mediating O *2p* states. Note that the states are not shown at the same intensity scale.

where $V_{ij}^{\alpha\beta}$ is the interaction energy when the sites i and j are occupied by the α and β atoms, respectively. The calculated parameters are negative and decay quickly as the Co$-$Co separation increases. This suggests a clustering tendency of the magnetic impurities in the semiconducting host.

In order to simulate annealing, we have used these parameters in Monte Carlo simulations of an Ising Hamiltonian described by

$$H = -\frac{1}{2}\sum_{i\neq j} V_{ij}\xi_i\xi_j,$$

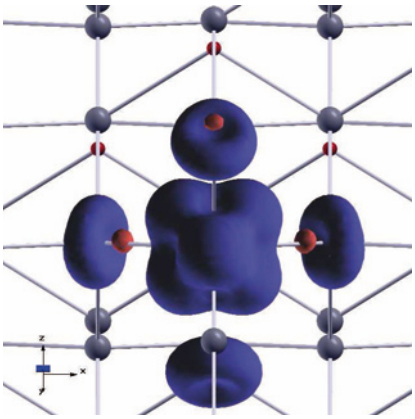

Figure 5.3: Magnetization density of a Co monomer in a ZnO matrix, evaluated within the LSDA+U for an energy interval of 0.2 eV below the Fermi level. Positive (negative) values of the magnetization density are represented in red (blue).

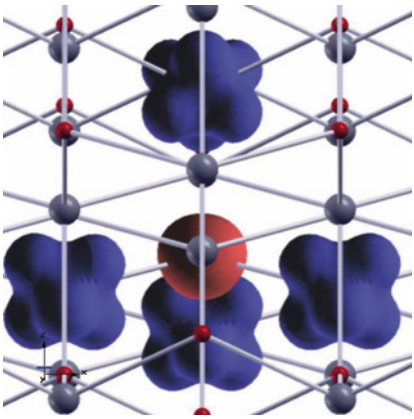

Figure 5.4: Same as in Fig. 5.3 but for a Co tetramer evaluated for an energy interval of 0.7 eV below the Fermi level.

where ξ_i is the occupation number at site i. Initially, the system is homogeneous. As the annealing time ($\sim$ Monte Carlo steps) increases, Co clusters start to develop in the system. The chemical distribution of the atoms strongly affects the magnetic behavior of the system, which turns from ferromagnetic to superparamagnetic as the number of Monte Carlo steps increases, as can be seen in Fig. 3 in Paper VI.

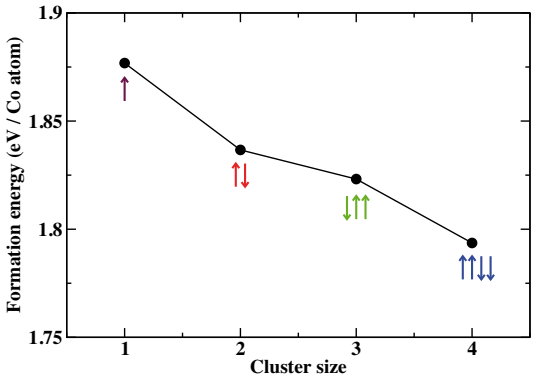

Figure 5.5: Formation energy as a function of the size of Co cluster for the corresponding ground state magnetic configurations.

6. (Co,Al)-doped ZnO

In Papers VII−VIII we extend our study of Co-doped ZnO by considering the additional doping of Al. The electronic structure, the chemical and magnetic interactions were investigated experimentally, as well as theoretically.

Thin films of 5% Co:ZnO and 5% Co, 0.8% Al:ZnO were prepared by solution-based methods, and further annealed in different conditions. The surface morphology and crystal structure were monitored by scanning electron microscopy (SEM) and X-ray diffraction (XRD). The electronic structure was experimentally studied by photoelectron spectroscopy (PES) and x-ray absorption spectroscopy (XAS). The magnetic properties were investigated by x-ray magnetic circular dichroism technique (XMCD) and using a superconducting quantum interference device (SQUID) magnetometer.

For the *ab initio* calculations, we have used both the PAW and the KKR-CPA methods. When using the PAW method, a wurtzite supercell was constructed to treat the disorder in the system introduced by the doping with Co and Al. The LSDA+U method was used for the exchange-correlation potential, where the Coulomb interaction parameter were chosen to be U = 9 and 5 eV, for the d bands of Zn, respectively Co. The exchange parameter J was set to 1 eV.

6.1 Electronic Structure

The calculated density of states is shown in Fig. 6.1(a)-(d). The valence bands consist of mainly O *2p* states. The Zn *3d* states are situated lower in energy, around 8 eV below the top of the valence band, which is in agreement with the experimental results obtained by photoemission spectroscopy. The occupied minority Co *3d* bands are located at the top of the valence band. It is important to mention that LSDA provides a wrong picture of the electronic structure: the Zn states are found to be much higher in energy, just below the O *2p* states; the band gap is much underestimated, and the occupied minority Co *3d* states are in the gap. This has a large impact on the sign as well as the strength of the magnetic interactions, as we have discussed in Paper V. Therefore, the effects of strong electron-electron interactions must be properly taken into account for a correct description of the system.

The effect of Al is to broaden slightly the Zn *3d* states, due to the hybridization with the Al states. In addition, the Fermi level becomes pinned at the

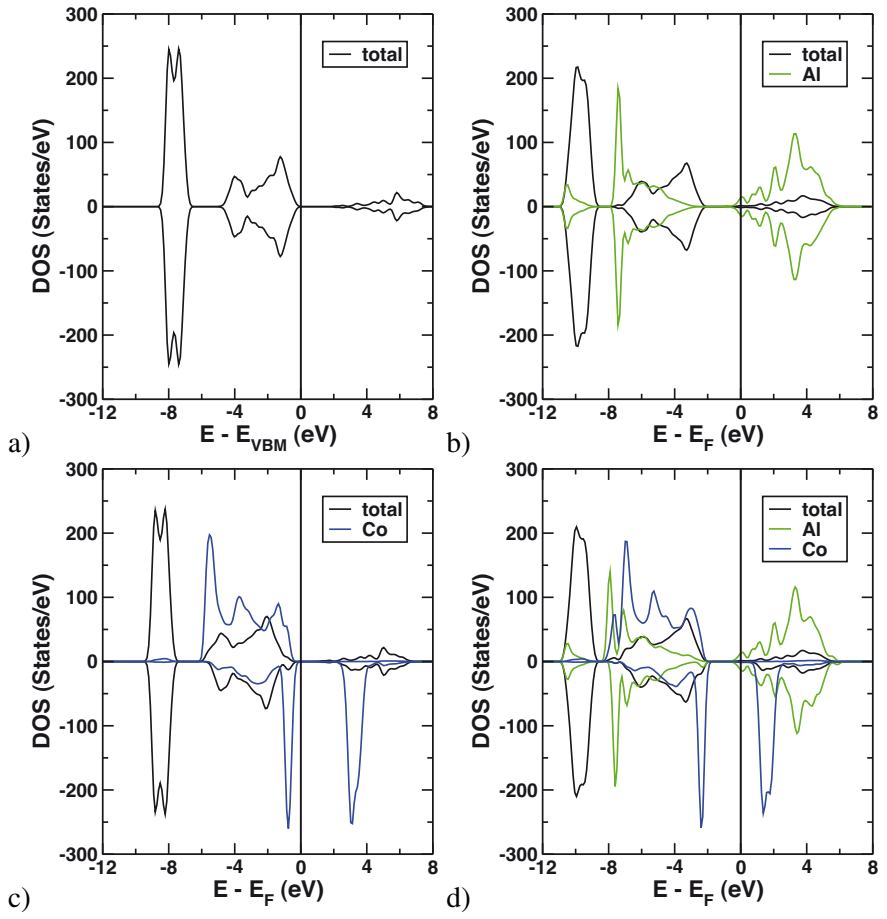

Figure 6.1: Calculated DOS for: (a) pure ZnO, (b) 1% Al:ZnO, (c) 5% Co:ZnO, (d) 5% Co, 1%Al:ZnO. The intensities of the Al and Co states are scaled to higher values.

bottom of the conduction band, the semiconductor thus becomes *n*-type. The Co states are pushed down in energy with respect to the valence band. This is caused by the appearance of a Co peak at the bottom of the valence band with Al co-doping. This shift of the Co states towards lower energies was observed in the photoemission spectra as well (*see* Fig. 7 in Paper VII).

6.2 Chemical and Magnetic Interactions

In order to study the chemical interactions among the Co atoms, we have used the Korringa-Kohn-Rostoker method together with the coherent potential approximation in order to treat disorder in the system. The chemical pair interactions were evaluated by the generalized perturbation method. The calculated

chemical interactions are negative, which suggests a clustering tendency of the Co atoms. As Al is introduced in the system, the strength of the interactions increases further, which suggests that the Co atoms prefer to cluster even more. We therefore envision that the experimental situation corresponds to the formation of Co clusters. Inside these, the magnetic interactions among the Co atoms are antiferromagnetic. This situation is best described as superparamagnetic.

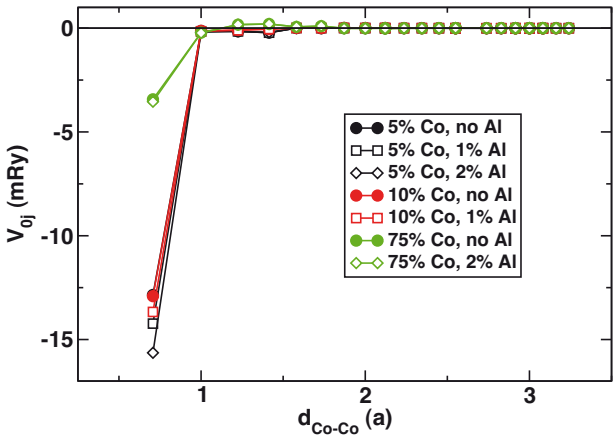

Figure 6.2: Calculated chemical pair-interactions versus Co-Co separation for different Co concentrations, and in the presence and absence of $\mathrm{Al_{Zn}}$.

7. $Fe_{81}Ni_{19}$/Co(001) Superlattices

The magnetic anisotropy and the structure of magnetic domains in bcc $Fe_{81}Ni_{19}/Co(001)$ superlattices were investigated in Paper IX. The magnetic anisotropy of thin films consists of two contributions. One of them is the shape anisotropy and it is comes from the long-ranged dipolar interactions. The other contribution is due to spin-orbit effects and it corresponds to the magneto-crystalline anisotropy, which in turn, consists of the bulk and interface anisotropies. A lot of the interesting physics regarding thin films comes from the competition between the different anisotropies.

Measurements using the magneto-optical Kerr effect and magnetic force microscopy indicate that the magnetization rotates from in-plane to out-of-plane as the thickness of the thin films increases from 85 to 1370 nm. The tilting angle of the magnetization with respect to the in-plane direction increases as the thickness increases.

Magnetic force microscopy images (*see* Fig. 7.1) show the well-ordered magnetic domain patterns, where the magnetization alternates from up to down. The patterns are typical for perpendicular anisotropy films. The formation of the domains can be understood from the competition between the exchange energy, which favors the parallel alignment of the neighboring spins, and the dipolar energy, which favors long-ranged antiferromagnetic alignment. The period of the domains increases nonlinearly as the thickness of the superlattices increases.

The behavior was captured qualitatively by a parametrized model for the magnetization. However, the solution of the linearized Landau-Lifshitz equation further improved the agreement with the experiments.

Paper X is a continuation of the studies on the bcc $Fe_{81}Ni_{19}/Co(001)$ superlattices. By magneto-optical Kerr effect and magnetic force microscopy measurements, a magnetization reorientation transition was found as the interface density varies. From combined *ab initio* calculations and analysis of the Landau-Lifshitz equation we explained that the transition is driven by the competition between the interface in-plane and the uniaxial bulk out-of-plane anisotropies.

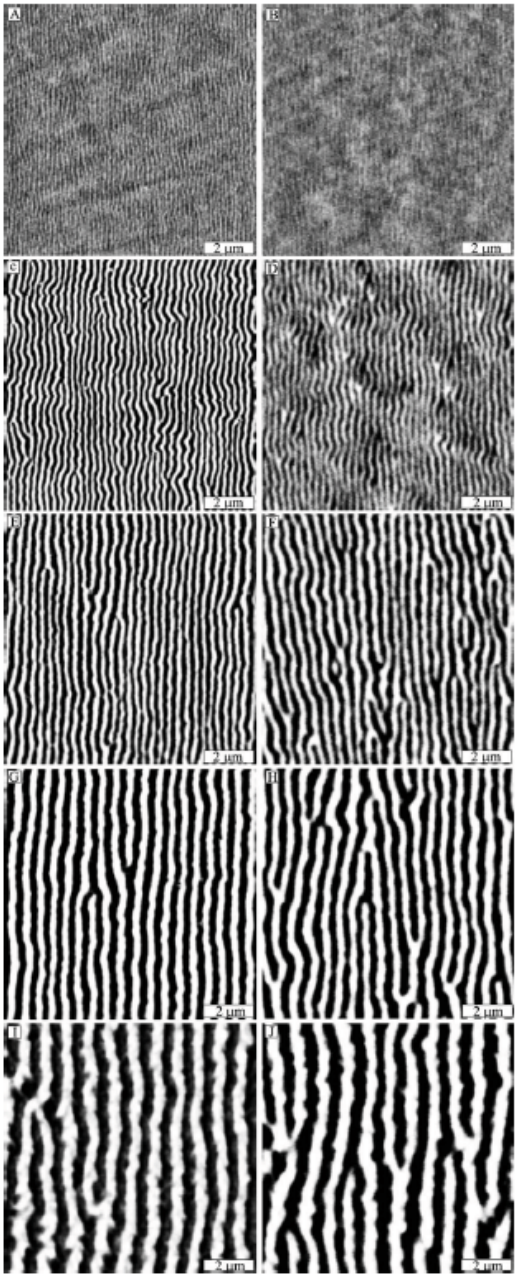

Figure 7.1: The MFM images obtained in zero applied field of bcc $Fe_{81}Ni_{19}/Co$ superlattices in the as-deposited state for (a) 25 bilayers (BL), (c) 50 BL, (e) 100 BL, (g) 200 BL, and (i) 400 BL and in-plane remanent states (b), (d), (f), (h), and (j), respectively.

8. Conclusions & Outlook

Dilute magnetic semiconductors have represented a hot topic of research for quite a few years now. Although thousands of articles have been dedicated to the subject, its main question, whether it is possible to realize a dilute magnetic semiconductor which is ferromagnetic at room temperature, remains unanswered. Among DMS, the most puzzling group seems to be the one of transition metal (TM)-doped wide band gap semiconductors, such as TM-doped GaN or ZnO.

Let us take Mn and Co-doped ZnO as examples. From *ab initio* calculations it is found that the pair exchange interactions decrease rapidly with the separation among the magnetic impurities. This is typical for a TM-doped wide band gap semiconductor for which the TM states lie in the band gap. The short ranged character of the magnetic interactions, combined with a low concentration of magnetic impurities, results in transition temperatures far below room temperature. A possible avenue would be digital ferromagnetic heterostructures or similar structures where the concentration of magnetic impurities is high locally.

One of the challenges of the *ab initio* community is to correctly describe the electronic structure of these materials. It is well known that LDA usually underestimates the band gap. As a consequence, the position of the impurity levels with respect to the host bands could be incorrectly described as well. These shortcomings can be improved by using the LDA+U method, or by using even more advanced methods, such as dynamical mean field theory (DMFT). In order to attest which is the best method to describe the system, comparisons with photoemission data from clean experiments should be made.

Experimentally there seems to be a great discord, as different results have been obtained by different groups. Sometimes this is due to different growth techniques, but at other times it is due to different interpretations. The challenges are great, and they are partly due to the fact that the magnetic signal of the sample is low, partly because not all techniques are sensitive enough to detect the presence of secondary phases. If these secondary phases are magnetic, the magnetic signal of the total sample could be misinterpreted.

For now, there is no such thing as a super magnifying glass that could penetrate deep into the material and determine the distribution of the magnetic atoms, possible defects or distortions in the local structure. Such information would be indeed very useful as input to *ab initio* and model calculations. Probably in a more distant future this will be possible.

From the theoretical point of view, it would be very interesting to simulate the growth of DMS, using kinetic Monte Carlo methods for example. With a better knowledge of the distribution of the magnetic atoms, the pair exchange interactions and the transition temperature can be determined in a more accurate way.

The field of dilute magnetic semiconductors is still open. Although progress might seem slow when it comes to some systems, the possibilities have not been exhausted. Carefully chosen additional dopants or defects, and why not, materials with metastable structures or grains with magnetic boundaries could be the answer to the long sought question. The future will tell.

Sammanfattning på Svenska

Densitetsfunktionalteori tillämpad på spinntronikmaterial

Konventionella elektronikkomponenter bygger på elektronisk transport av laddningsbärare, elektronerna, genom en halvledare, oftast baserad på kisel. Spinntroniken strävar i stället efter att använda både elektronernas laddning och deras spinn, och därmed överbrygga gapet mellan industrierna för halvledare och magnetisk lagring. Detta ger en ny generation komponenter som trots att de är mindre kan hantera mer information än de konventionella.

Startskottet för spinntroniken var när Albert Fert och Peter Grünberg 1988 upptäckte den gigantiska magnetoresistaseffekten (GMR), en upptäckt som sedan belönades med Nobelpriset år 2007. Effekten består i en mycket stor förändring i det elektriska motståndet när materialet befinner sig i ett magnetisk fält, vilket beror på att elektronernas transportegenskaper är spinnberoende. Det tog mindre än tio år innan upptäckten började utnyttjas i datorindustrin. Idag finns persondatorer överallt, deras storlek har minskat och hastigheten ökat samtidigt som priserna stått stilla. Detta, tillsammans med internet, påverkar hur vi arbetar, använder våra telefoner och överhuvud taget interagerar med varandra. Men att beskriva det vore en hel avhandling i sig.

Utspädda magnetiska halvledare (eng. dilute magnetic semiconductors, DMS) är en grupp material som på senare tid har blivit intressant i spinntroniken. Som namnet antyder består dom av ett halvledande värdmaterial i vilket man introducerat små mängder magnetiska orenheter. I Figur 8.1 skisseras hur ett sådant material kan se ut. Det som i första hand eftersträvas är ett DMS-material där de magnetiska momenten är i ett ordnat tillstånd vid rumstemperatur.

Ett framsteg kom 1992 då Hideo Ohno och hans medarbetare upptäckte ferromagnetism i indiumarsenid dopad med bara 1.3% mangan [1]. Några år senare, 1996, fann de ferromagnetisk ordning också i mangandopad galliumarsenid, med en ordningstemperatur på 110 K [2]. Senare arbeten har rapporterat ordningstemperaturer upp till 173 K [3], i skrivande stund förmodligen det högsta, ej ifrågasatta, värdet för denna klass av material. Tomasz Dietl genomförde studier som fick stort genomslag när han med hjälp av en teoretisk modell förutsade ordningstemperaturen för en serie mangandopade halvledare [4]. Enligt modellen, skulle mangandopad zinkoxid eller galliumnitrid ha ferromagnetiska ordningstemperaturer så höga som 300 K. Dessa resultat ledde till ett väldigt intresse för dessa material — tusentals artiklar har publicerats

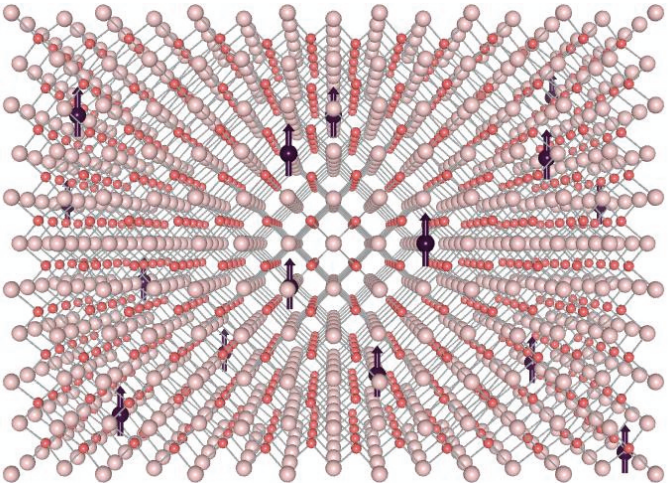

Figure 8.1: Schematisk representation av en utspädd magnetisk halvledare.

och antalet bara stiger. Trots detta kvarstår kontroverserna om de magnetiska egenskaperna för de utspädda magnetiska halvledarna och man har inte uppnått koncensus om att ordningstemperaturer över rumstemperatur faktiskt har uppnåtts.

I den här avhandlingen behandlas magnetismen i utspädda magnetiska halvledare med hjälp av *ab initio* metoder, mer specifikt densitetsfunktionalteori (DFT), som har använts för att bestämma materialegenskaper. DFT transformerar det komplicerade mångkropparsproblemet för elektronerna till en enklare form som bara kräver kunskap om elektronernas rumsliga fördelning. Grunden till DFT lades av Pierre Hohenberg och Walter Kohn 1964. Den blev snart en mycket populär teknik och har sedan dess framgångsrikt använts för beräkningar av en lång rad material. För metodens mångsidighet belönades en av upphovsmännen, Walter Kohn, med nobelpriset i kemi 1998. Vi kombinerar DFT med Monte Carlo-simuleringar för att studera materialegenskaper vid olika temperaturer. Genom att studera hur magnetiseringen varierar med temperatur kan ordningstemperaturen för systemet bestämmas.

Här följer en sammanfattning av avhandlingens huvudsakliga resultat.

Hur den magnetiska växelverkan i Mn-dopad ZnO påverkas av defekter har undersökts. I frånvaro av defekter är växelverkan mellan manganatomerna liten och antiferromagnetisk. Donatordefekter, som syrevakanser och interstitiella zinkatomer, ökar den antiferromagnetiska växelverkan, medan acceptordefekter, som zinkvakanser eller substitution av kväve på syrepositioner, ger ferromagnetisk växelverkan. För små koncentrationer av Mn ($\sim 5\%$) är ordningstemperaturen för systemet låg på grund av den korta räckvidden för utbytesväxelverkan och effekter från systemets oordning.

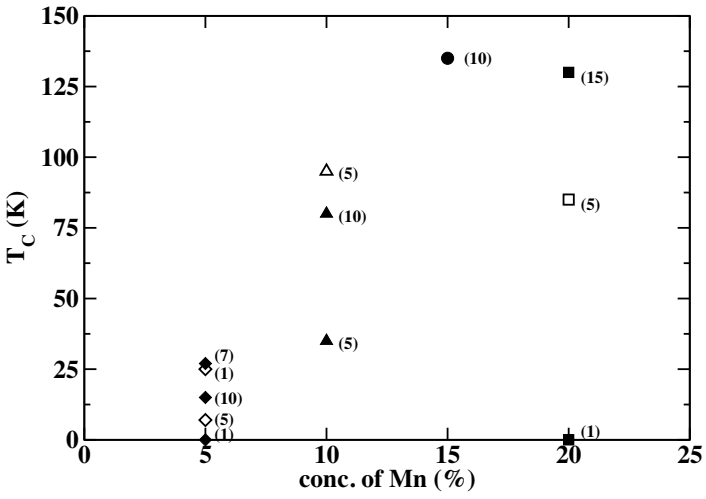

Figure 8.2: Beräknade curietemperaturer från Monte Carlo-simuleringar. Fyllda symboler svarar mot kvävesubstitution och öppna symboler mot zinkvakanser. Defektkoncentrationen är angiven inom parentes.

Högre värden (exempelvis 135 K) kan fås genom att finjustera mangan- och defekt-koncentrationerna. Ett diagram som sammanfattar resultaten visas i Figur 8.2.

Lokala effekter i kristallstrukturen, som Co-atomers tendens att bilda kluster i ZnO-matrisen undersöktes. Elektronstrukten, och därmed den magnetiska växelverkan mellan Co-atomerna är starkt beroende på vilken utbytes-korrelations-funktional som används. Vi finner att koboltorenheterna tenderar att bilda nanokluster och deras växelverkan är antiferromagnetisk, beräknad med den lokala densitets-approximationen (LDA) + Hubbard U.

Elektronstruktur och den kemiska och magnetiska växelverkan i Co och (Co,Al)-dopad ZnO undersöktes med experimentella och teoretiska tekniker. Elektronstrukturen har Co-tillstånd som ligger vid toppen av valensbandet. Al-dopningen sätter Ferminivån vid botten av ledningsbandet, vilket är det normala för en n-dopad halvledare. För bra överensstämmelse mellan experiment och experiment krävs approximationer som går utöver LDA. Vi finner att Co-atomerna tenderar att bilda kluster inom halvledarmatrisen och att denna effekt ökar av Al-dopningen. Detta i kombination med att den magnetiska växelverkan mellan Co-orenheterna är antiferromagnetisk antyder att systemet bäst kan beskrivas som superparamagnetiskt.

Den magnetiska anisotropin och utvecklingen av magnetiska domäner i $Fe_{81}Ni_{19}$/Co(001)supergitter har studerats både experimentellt och med spinndynamik. En magnetisk reorienteringsövergång upptäcktes. Dessa material har viktiga tillämpningar som magnetooptiska inspelningsmedier.

Acknowledgements

Although I'll soon have finished my PhD, it feels as if I've started just yesterday. Memories come racing from the past to the point I wish it had lasted a bit longer. But it is a journey that had made me encounter wonderful people, and I am grateful for that.

Thank you, Olle, and thank you, Biplab, for all the support during these years and for the patience of answering my questions, even if asked for a second time. Thanks to all the seniors, who, through their presence in the group, have made it such a rich working environment. Thank you for the courses you gave or simply for sharing your experience whenever needed. Thanks to Elisabeth for all the help with the practical details.

My gratitude to Voicu Crişan for introducing me to the *ab initio* world. I'd like to thank Mebarek Alouani for our collaboration on transport properties of multilayers. My thanks to Josef Kudrnovský for all the useful discussions on DMS and to Silvia Picozzi and Kunihiko Yamauchi for our collaboration on multiferroics. Thanks to all the experimentalists I had the opportunity to work with, it was a pleasure. I would also like to thank Mukul for our work on clusters, and to Nadjib for all the discussions about DFT.

Thanks to the postdoc gang, as I like to call it, Seb, Roberto, Andreia, and Ralph, it is always nice to hang out with you. Thank you Pooja for all the laughters we had together and for cooking all that great food for us (guess who was doing nothing?). Thanks to Maria for the baking sessions and to Suparna for the nice parties. I got to hear amazing ghost stories at your place! Thanks to Younsuk, Martin, Karel, Sergiu, Moyses, Dominik, Mikael, Petros, Duck Young, Jan, Oleg, Torbjörn, Oscar, Carlos, Patrik, Fredrik, and all of you, for all the time we have spent together, whether it was fika, movie nights, parties, excursions ...

I'd like to thank my parents, for encouraging me to come abroad, and my little sister for all her help. I'd also like to thank Inga and Lars, for being wonderful to me, and to my *extended* family. Special thanks to Ilie for designing the cover, it looks great! Thanks to Seb for reading the thesis and to Torbjörn for helping me with the translation.

My warmest thanks (*şi o mie de pupici*) to Johan, who almost finished before me, may we fight for grants forever!

Bibliography

[1] H. Ohno, H. Munekata, T. Penney, S. Von Molnár, and L. L. Chang. Magneto-transport properties of *p*-type (In,Mn)As diluted magnetic III-V semiconductors. *Phys. Rev. Lett.*, 68(17):2664–2667, Jan 1992.

[2] H. Ohno. Making nonmagnetic semiconductors ferromagnetic. *Science*, 281(5379):951–956, Jan 1998.

[3] T. Jungwirth, K.Y. Wang, J. Mašek, K.W. Edmonds, J. König, J. Sinova, M. Polini, N.A. Goncharuk, A.H. MacDonald, M. Sawicki, A.W. Rushforth, R.P. Campion, L.X. Zhao, C.T. Foxon, and B.L. Gallagher. Prospects for high temperature ferromagnetism in (Ga,Mn)As semiconductors. *Phys. Rev. B*, 72(16):165204, Jan 2005.

[4] T. Dietl, H. Ohno, F. Matsukura, J. Cibert, and D. Ferrand. Zener model description of ferromagnetism in zinc-blende magnetic semiconductors. *Science*, 287(5455):1019–1022, Jan 2000.

[5] M. Born and R. Oppenheimer. Quantum theory of molecules. *Ann. Phys.-Berlin*, 84(20):0457–0484, Jan 1927.

[6] P. Hohenberg and W. Kohn. Inhomogeneous electron gas. *Phys. Rev.*, 136(3B):B864–B871, Nov 1964.

[7] W. Kohn and L. Sham. Self-consistent equations including exchange and correlation effects. *Phys. Rev.*, 140(4A):A1133–A1138, Nov 1965.

[8] U. von Barth and L. Hedin. A local exchange-correlation potential for the spin polarized case. i. *Journal of Physics C: Solid State Physics*, 5:1629, Jul 1972.

[9] J. Slater. A simplification of the Hartree-Fock method. *Phys. Rev.*, 81(3):385–390, Feb 1951.

[10] D. Ceperley and B. Alder. Ground state of the electron gas by a stochastic method. *Phys. Rev. Lett.*, 45(7):566–569, Aug 1980.

[11] S.H. Vosko, L. Wilk, and M. Nusair. Accurate spin-dependent electron liquid correlation energies for local spin-density calculations - A critical analysis. *Can. J. Phys.*, 58(8):1200–1211, Jan 1980.

[12] John Perdew and Yue Wang. Accurate and simple analytic representation of the electron-gas correlation energy. *Phys. Rev. B*, 45(23):13244–13249, Jun 1992.

[13] John Perdew, J. Chevary, S. Vosko, Koblar Jackson, Mark Pederson, D. Singh, and Carlos Fiolhais. Atoms, molecules, solids, and surfaces: Applications of the generalized gradient approximation for exchange and correlation. *Phys. Rev. B*, 46(11):6671–6687, Sep 1992.

[14] J.P. Perdew. Orbital functional for exchange and correlation - Self-interaction correction to the local density approximation. *Chem. Phys. Lett.*, 64(1):127–130, Jan 1979.

[15] A. Zunger, J.P. Perdew, and G.L. Oliver. A self-interaction corrected approach to many-electron systems - Beyond the local spin-density approximation. *Solid State. Commun.*, 34(12):933–936, Jan 1980.

[16] A. Svane. Electronic structure of cerium in the self-interaction corrected local spin density approximation. *Phys. Rev. Lett.*, 72(8):1248–1251, Feb 1994.

[17] Vladimir Anisimov, Jan Zaanen, and Ole Andersen. Band theory and Mott insulators: Hubbard U instead of Stoner I. *Phys. Rev. B*, 44(3):943–954, Jul 1991.

[18] P. Blöchl. Projector augmented-wave method. *Phys. Rev. B*, 50(24):17953–17979, Dec 1994.

[19] G. Kresse and D. Joubert. From ultrasoft pseudopotentials to the projector augmented-wave method. *Phys. Rev. B*, 59(3):1758–1775, Jan 1999.

[20] G. Kresse and J. Furthmüller. Efficient iterative schemes for *ab initio* total-energy calculations using a plane-wave basis set. *Phys. Rev. B*, 54(16):11169–11186, Oct 1996.

[21] J. Korringa. On the calculation of the energy of a bloch wave in a metal. *Physica*, 13(6-7):392–400, Jan 1947.

[22] W. Kohn and N. Rostoker. Solution of the Schrödinger equation in periodic lattices with an application to metallic lithium. *Phys. Rev.*, 94(5):1111–1120, Jan 1954.

[23] O.K. Andersen. Simple approach to the band-structure problem. *Solid State Commun.*, 13(2):133–136, Jan 1973.

[24] O. Andersen. Linear methods in band theory. *Phys. Rev. B*, 12(8):3060–3083, Oct 1975.

[25] I. Turek, V. Drchal, J. Kudrnovsky, M. Sob, and P. Weinberger. *Electronic Structure of Disordered Alloys, Surfaces, and Interfaces*. Kluwer Academic Publishers, 1997.

[26] Paul Soven. Coherent-potential model of substitutional disordered alloys. *Phys. Rev.*, 156(3):809–813, Apr 1967.

[27] D. Taylor. Vibrational properties of imperfect crystals with large defect concentrations. *Phys. Rev.*, 156(3):1017–1029, Apr 1967.

[28] B. Velický, S. Kirkpatrick, and H. Ehrenreich. Single-site approximations in the electronic theory of simple binary alloys. *Phys. Rev.*, 175(3):747–766, Nov 1968.

[29] A. Gonis and J. Garland. Multishell method: Exact treatment of a cluster in an effective medium. *Phys. Rev. B*, 16(6):2424–2436, Sep 1977.

[30] N. Mermin. Thermal properties of the inhomogeneous electron gas. *Phys. Rev.*, 137(5A):A1441–A1443, Mar 1965.

[31] I. Turek, J. Kudrnovský, V. Drchal, and P. Bruno. Exchange interactions, spin waves, and transition temperatures in itinerant magnets. *Philos. Mag.*, 86(12):1713–1752, Jan 2006.

[32] M. Pajda, J. Kudrnovský, I. Turek, V. Drchal, and P. Bruno. Ab initio calculations of exchange interactions, spin-wave stiffness constants, and Curie temperatures of Fe, Co, and Ni. *Phys. Rev. B*, 64(17):174402, Oct 2001.

[33] A.I. Liechtenstein, M.I. Katsnelson, V.P. Antropov, and V.A. Gubanov. Local spin-density functional-approach to the theory of the exchange interactions in ferromagnetic metals and alloys. *J. Magn. Magn. Mater.*, 67(1):65–74, Jan 1987.

[34] A. Oswald, R. Zeller, P.J. Braspenning, and P.H. Dederichs. Interaction of magnetic impurities in Cu and Ag. *Journal of Physics F: Metal Physics*, 15:193, Jan 1985.

[35] O.K. Andersen, H.L. Skriver, H. Nohl, and B. Johansson. Electronic-structure of transition-metal compounds; Ground-state properties of the 3d-monoxides in the atomic sphere approximation. *Pure Appl. Chem.*, 52(1):93–118, Jan 1980.

[36] S. Halilov, H. Eschrig, A. Perlov, and P. Oppeneer. Adiabatic spin dynamics from spin-density-functional theory: Application to Fe, Co, and Ni. *Phys. Rev. B*, 58(1):293–302, Jul 1998.

[37] L. Sandratskii and P. Bruno. Exchange interactions and Curie temperature in (Ga,Mn)As. *Phys. Rev. B*, 66(13):134435, Oct 2002.

[38] Raza Tahir-Kheli and H. Jarrett. Ferromagnetic Curie temperature in cubic lattices with next-nearest-neighbor interaction. *Phys. Rev.*, 135(4A):A1096–A1098, Aug 1964.

[39] D.P. Landau and K. Binder. *A Guide to Monte Carlo Simulations in Statistical Physics*. Cambridge University Press, Cambridge, England, 2000.

[40] S. Kolesnik and B. Dabrowski. Absence of room temperature ferromagnetism in bulk Mn-doped ZnO. *J. Appl. Phys.*, 96(9):5379–5381, Jan 2004.

[41] X.M. Cheng and C.L. Chien. Magnetic properties of epitaxial Mn-doped ZnO thin films. *J. Appl. Phys.*, 93(10):7876–7878, Jan 2003.

[42] T. Fukumura, Z.W. Jin, M. Kawasaki, T. Shono, T. Hasegawa, S. Koshihara, and H. Koinuma. Magnetic properties of Mn-doped ZnO. *Appl. Phys. Lett.*, 78(7):958–960, Jan 2001.

[43] S.W. Jung, S.-J. An, G.-C. Yi, C.U. Jung, S.-I. Lee, and S. Cho. Ferromagnetic properties of Zn1-xMnxO epitaxial thin films. *Appl. Phys. Lett.*, 80(24):4561–4563, Jan 2002.

[44] P. Sharma, A. Gupta, K.V. Rao, F.J. Owens, R. Sharma, R. Ahuja, J.M.O. Guillen, B. Johansson, and G.A. Gehring. Ferromagnetism above room temperature in bulk and transparent thin films of Mn-doped ZnO. *Nat. Mater.*, 2(10):673–677, Jan 2003.

[45] A.K. Pradhan, K. Zhang, S. Mohanty, J.B. Dadson, D. Hunter, J. Zhang, D.J. Sellmyer, U.N. Roy, Y. Cui, S. Mathews, B. Joseph, B.R. Sekhar, and B.K. Roul. High-temperature ferromagnetism in pulsed-laser deposited epitaxial (Zn,Mn)O thin films: Effects of substrate temperature. *Appl. Phys. Lett.*, 86(15):152511, Jan 2005.

[46] F. Haldane and P. Anderson. Simple model of multiple charge states of transition-metal impurities in semiconductors. *Phys. Rev. B*, 13(6):2553–2559, Mar 1976.

[47] E. Chikoidze, Y. Dumont, F. Jomard, D. Ballutaud, P. Galfier, O. Gorochov, and D. Ferrand. Semiconducting and magnetic properties of Zn1-xMnxO films grown by metalorganic chemical vapor deposition. *J. Appl. Phys.*, 97(10):10D327, Jan 2005.

[48] S.W. Yoon, S.B. Cho, S.C. We, S. Yoon, B.J. Suh, H.K. Song, and Y.J. Shin. Magnetic properties of ZnO-based diluted magnetic semiconductors. *J. Appl. Phys.*, 93(10):7879–7881, Jan 2003.

[49] E. Chikoidze, H.J. von Bardeleben, Y. Dumont, P. Galtier, and J.L. Cantin. Magnetic interactions in Zn1-xMnxO studied by electron paramagnetic resonance spectroscopy. *J. Appl. Phys.*, 97(10):10D316, Jan 2005.

[50] Y. Ma, G.T. Du, S.R. Yang, Z.T. Li, B.J. Zhao, X.T. Yang, T.P. Yang, Y.T. Zhang, and D.L. Liu. Control of conductivity type in undoped ZnO thin films grown by metalorganic vapor phase epitaxy. *J. Appl. Phys.*, 95(11):6268–6272, Jan 2004.

[51] H. Akai. Ferromagnetism and its stability in the diluted magnetic semiconductor (In, Mn)As. *Phys. Rev. Lett.*, 81(14):3002–3005, Oct 1998.

[52] John Perdew, Kieron Burke, and Matthias Ernzerhof. Generalized gradient approximation made simple. *Phys. Rev. Lett.*, 77(18):3865–3868, Oct 1996.

[53] S.L. Dudarev, G.A. Botton, S.Y. Savrasov, C.J. Humphreys, and A.P. Sutton. Electron-energy-loss spectra and the structural stability of nickel oxide: An LSDA+U study. *Phys. Rev. B*, 57(3):1505–1509, Jan 1998.

[54] X. Cui, J. Medvedeva, B. Delley, A. Freeman, N. Newman, and C. Stampfl. Role of embedded clustering in dilute magnetic semiconductors: Cr doped GaN. *Phys. Rev. Lett.*, 95(25):256404, Dec 2005.

[55] F. Ducastelle. *Order and Phase Stability in Alloys*. North-Holland, Amsterdam, 1991.

Acta Universitatis Upsaliensis

Digital Comprehensive Summaries of Uppsala Dissertations from the Faculty of Science and Technology 721

Editor: The Dean of the Faculty of Science and Technology

A doctoral dissertation from the Faculty of Science and Technology, Uppsala University, is usually a summary of a number of papers. A few copies of the complete dissertation are kept at major Swedish research libraries, while the summary alone is distributed internationally through the series Digital Comprehensive Summaries of Uppsala Dissertations from the Faculty of Science and Technology. (Prior to January, 2005, the series was published under the title "Comprehensive Summaries of Uppsala Dissertations from the Faculty of Science and Technology".)

Distribution: publications.uu.se
urn:nbn:se:uu:diva-119887

ACTA
UNIVERSITATIS
UPSALIENSIS
UPPSALA
2010